Cell Reports
Medicine

Article

Aurora A kinase inhibition induces accumulation of SCLC tumor cells in mitosis with restored interferon signaling to increase response to PD-L1

Graphical abstract

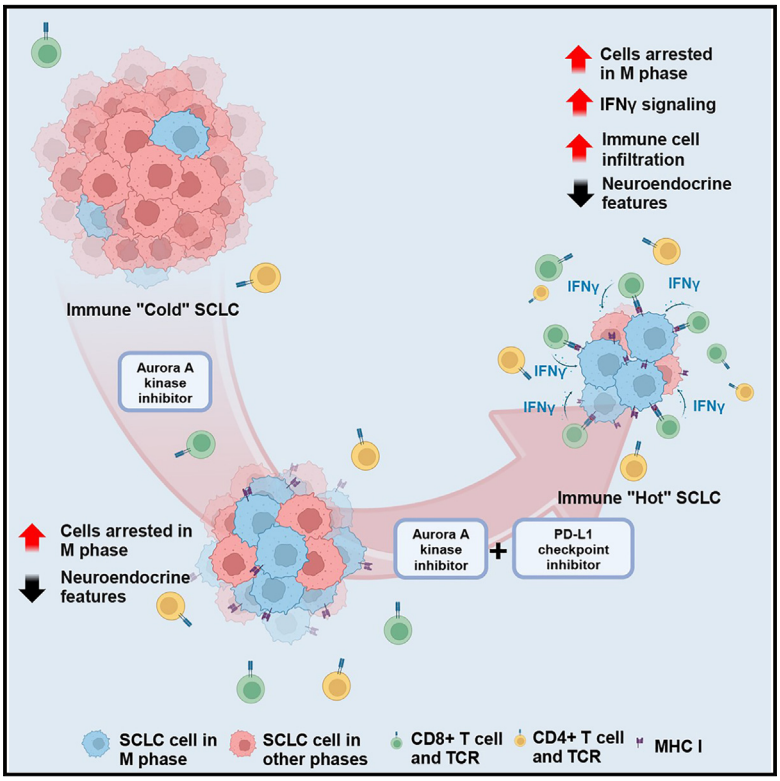

Highlights

- Aurora A kinase inhibition + PD-L1 immunotherapy has durable efficacy in SCLC mouse models
- LSN3321213 and PD-L1 increases T-lymphocyte infiltration in tumors
- LSN3321213 blocks tumor cells in mitosis with high interferon signaling and MHC class I

Authors

Yixiang Li, Navin R. Mahadevan, Leslie Duplaquet, ..., Prafulla C. Gokhale, Quang-De Nguyen, Matthew G. Oser

Correspondence

matthew_oser@dfci.harvard.edu

In brief

Li et al. show that Aurora A kinase inhibition causes accumulation of SCLC tumor cells in mitosis with high expression of antigen-presentation genes mimicking an immunotherapy-responsive inflamed tumor cell state. This promotes T-lymphocyte infiltration, and Aurora A kinase inhibition + PD-L1 has durable efficacy in immunocompetent SCLC mouse models.

Li et al., 2023, Cell Reports Medicine *4*, 101282
November 21, 2023
https://doi.org/10.1016/j.xcrm.2023.101282

CellPress

Cell Reports Medicine

CellPress
OPEN ACCESS

Article

Aurora A kinase inhibition induces accumulation of SCLC tumor cells in mitosis with restored interferon signaling to increase response to PD-L1

Yixiang Li,[1] Navin R. Mahadevan,[1,2] Leslie Duplaquet,[1] Deli Hong,[1] Yavuz T. Durmaz,[1] Kristen L. Jones,[1,3] Hyeonseo Cho,[1] Murry Morrow,[1,3] Andrea Protti,[1,3] Michael J. Poitras,[1,4,5] Benjamin F. Springer,[1,4,5] Roderick T. Bronson,[6] Xueqian Gong,[7] Yu-Hua Hui,[7] Jian Du,[7] Jackson Southard,[1,8] Tran Thai,[1] Shuqiang Li,[1,8] Patrick H. Lizotte,[1,4] Prafulla C. Gokhale,[1,4,5] Quang-De Nguyen,[1,3] and Matthew G. Oser[1,9,10,*]

[1]Department of Medical Oncology, Dana-Farber Cancer Institute and Brigham and Women's Hospital, Harvard Medical School, Boston, MA 02215, USA
[2]Department of Pathology, Brigham and Women's Hospital, Boston, MA 02115, USA
[3]Lurie Family Imaging Center, Center for Biomedical Imaging in Oncology, Dana-Farber Cancer Institute, Boston, MA 02210, USA
[4]Belfer Center for Applied Cancer Science, Dana-Farber Cancer Institute, Boston, MA 02215, USA
[5]Experimental Therapeutics Core, Dana-Farber Cancer Institute, Boston, MA 02210, USA
[6]Division of Immunology, Department of Microbiology and Immunobiology, Harvard Medical School, Boston, MA 02215, USA
[7]Loxo@Lilly, Indianapolis, IN 46225, USA
[8]Translational Immunogenomics Lab, Dana Farber Cancer Institute, Boston, MA, USA
[9]Department of Medicine, Brigham and Women's Hospital, Harvard Medical School, Boston, MA 02115, USA
[10]Lead contact
*Correspondence: matthew_oser@dfci.harvard.edu
https://doi.org/10.1016/j.xcrm.2023.101282

SUMMARY

Despite small cell lung cancers (SCLCs) having a high mutational burden, programmed death-ligand 1 (PD-L1) immunotherapy only modestly increases survival. A subset of SCLCs that lose their ASCL1 neuroendocrine phenotype and restore innate immune signaling (termed the "inflammatory" subtype) have durable responses to PD-L1. Some SCLCs are highly sensitive to Aurora kinase inhibitors, but early-phase trials show short-lived responses, suggesting effective therapeutic combinations are needed to increase their durability. Using immunocompetent SCLC genetically engineered mouse models (GEMMs) and syngeneic xenografts, we show durable efficacy with the combination of a highly specific Aurora A kinase inhibitor (LSN3321213) and PD-L1. LSN3321213 causes accumulation of tumor cells in mitosis with lower ASCL1 expression and higher expression of interferon target genes and antigen-presentation genes mimicking the inflammatory subtype in a cell-cycle-dependent manner. These data demonstrate that inflammatory gene expression is restored in mitosis in SCLC, which can be exploited by Aurora A kinase inhibition.

INTRODUCTION

Small cell lung cancer (SCLC) accounts for ~10%–15% of all lung cancers and is strongly associated with smoking.[1] Approximately two out of three patients present with incurable metastatic (extensive stage [ES]) disease with a median overall survival (OS) of only 10–12 months.[1] Until 2018, first-line treatment was combination platinum-etoposide chemotherapy, which has a high response rate of ~60%–70%, but its benefit is short lived and the disease recurs in almost all patients.[2] The Impower 133 and CASPIAN clinical trials showed a survival benefit of adding programmed death-ligand 1 (PD-L1) immune checkpoint blockade (ICB) to platinum-etoposide in the first-line setting, which led to US Food and Drug Administration (FDA) approval of platinum-etoposide + PD-L1 ICB.[3,4] However, the added benefit of PD-L1 ICB was modest, extending survival only by ~2 months,[3,4] and only a few patients had long-term durable benefit. This was surprising given that SCLC has a very high mutational burden,[5] suggesting SCLCs inherently harbor immune evasion mechanisms.

Major histocompatibility complex (MHC) class I antigen presentation on tumors cells is necessary for a robust anti-tumor immune response.[6,7] Defective MHC-I expression is a common resistance mechanism to programmed cell death protein 1 (PD-1)/PD-L1 ICB across many cancer types.[8] It has long been appreciated that SCLC tumor cells inherently silence MHC-I through functional repression of TAP1,[9] which compromises the ability of T cells to recognize and kill SCLC tumor cells and likely hinders responses to PD-1/PD-L1 ICB. Recent data show that MHC-I is silenced in ~85% of SCLC human patient samples.[10–12] Interestingly, ~15% of human SCLCs with lower expression of the neuroendocrine transcription factor (TF) ASCL1 have restored tumor cell MHC-I expression.[10] SCLC tumors with high tumor cell MHC-I derived significantly greater

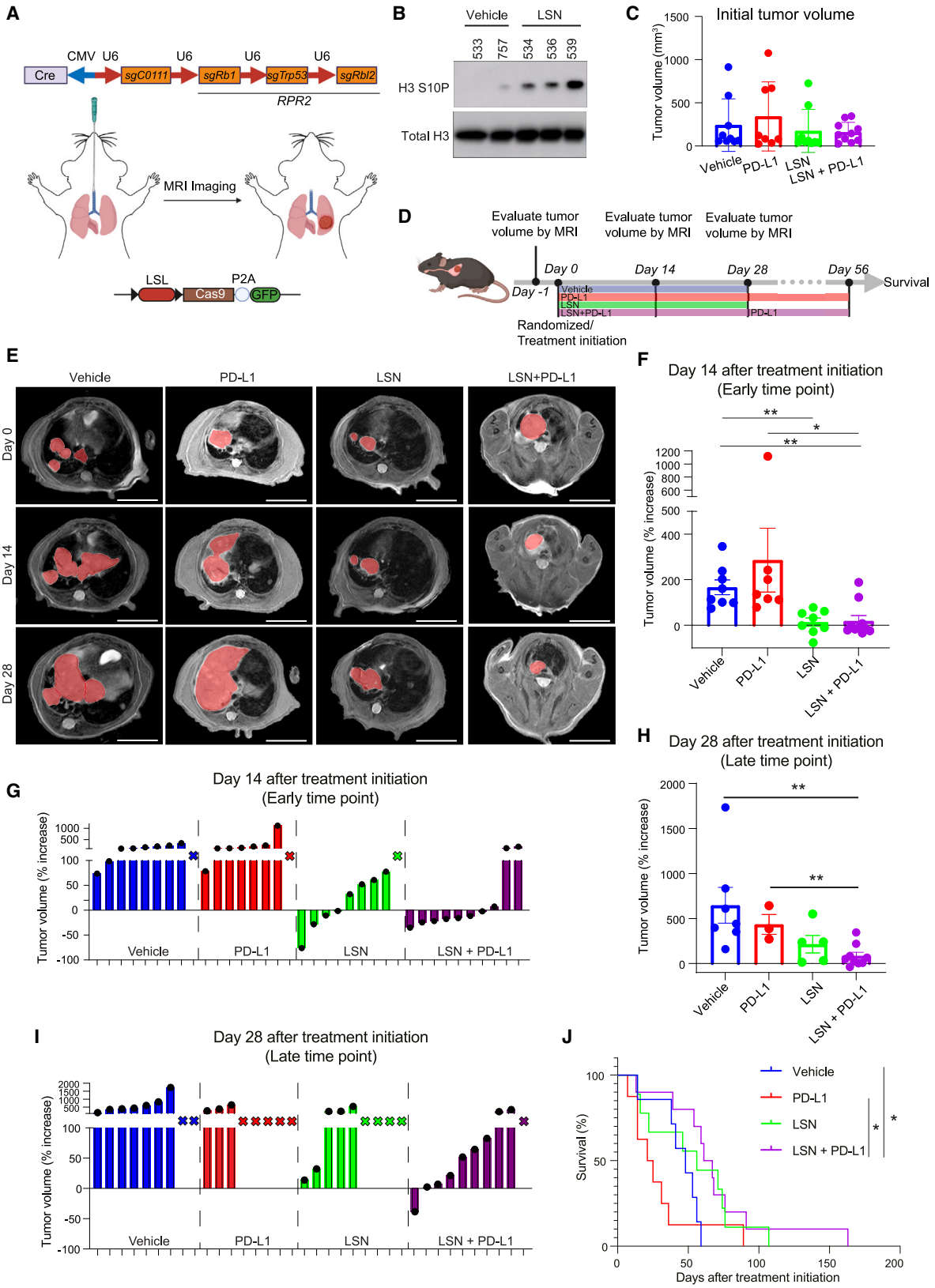

(legend on next page)

benefit from ICB,[10] which was recently validated as the most significant predictor of ICB responses in a larger study with 286 SCLC patient samples.[13] Similarly, a subset of SCLC patients whose tumors (1) lost expression of lineage TFs ASCL1, NEUROD1, and POU2F3; and (2) highly expressed genes involved in immune signaling gained significantly more benefit from ICB, leading to this subset of SCLC tumors being described as the "inflammatory" subtype.[14] Hence, enhancing MHC-I expression and inflammatory gene expression has potential to therapeutically restore SCLC's inherent immunogenicity, particularly in the neuroendocrine ASCL1 subtype that inherently silences MHC-I.[10]

Previous studies found that SCLCs are highly sensitive to Aurora A or B kinase inhibition (AURKAi or AURKBi),[15–20] which led to several clinical trials testing AURKAi or AURKBi in SCLC. Increased tumor cell-autonomous sensitivity to Aurora kinase inhibition in SCLC is due to at least two factors: (1) genetic loss of *RB1*, found in >90% of SCLCs, causes a hyper-dependency on AURKA or AURKB for their survival[15,16]; (2) high expression of MYC, which is overexpressed or amplified in some SCLCs, correlates with and is sufficient to induce sensitivity to AURKi in an *RB1*-mutant background.[17–20] Retrospective correlative studies from a phase II clinical trial testing the AURKi alisertib combined with paclitaxel vs. paclitaxel alone in SCLC patients support these findings, demonstrating a significant increase in progression-free survival (PFS) in patients with *RB1* pathway mutations or MYC expression in the alisertib + paclitaxel arm vs. paclitaxel alone.[21] Although statistically significant, the PFS benefit in patients with *RB1*-pathway mutations or MYC expression was modest, highlighting the need for combination strategies with AURKi to increase the durability of their response.

Given the hypersensitivity of SCLCs to AURKi but lack of durable activity in patients[21] and the modest overall efficacy of PD-L1 ICB in SCLC,[3,4] particularly in ASCL1-positive SCLCs, which silence MHC-I,[10,14] we hypothesized that AURKi would cooperate with PD-L1 to induce more meaningful durable antitumor efficacy. Here, we tested this hypothesis in immunocompetent SCLC mouse models using a highly selective AURKAi LSN3321213, the erbumine salt of LY3295668,[15] which is currently in a clinical trial for SCLC patients.

RESULTS

Combination treatment with the Aurora A kinase inhibitor LSN3321213 and PD-L1 has activity in an autochthonous immunocompetent small cell lung cancer mouse model

To study whether the highly specific AURKAi LSN3321213[15] potentiates the efficacy of PD-L1 ICB in SCLC, we used an SCLC CRISPR-based genetically engineered mouse model (GEMM).[22] In this GEMM, autochthonous SCLCs develop ~8–10 months after intratracheal (IT) injection of an adenovirus that encodes single guide RNAs (sgRNAs) targeting *Rb1*, *Trp53*, and *Rbl2* (referred to as *RPR2*) and Cre recombinase into Lox-Stop-Lox (LSL)-Cas9 congenic BL6J mice[22] (Figure 1A). We chose the *RPR2* GEMM for these studies as it forms SCLC tumors of the pure ASCL1 subtype, which comprises ~60% of human SCLCs,[25] and is associated with antigen-presentation silencing.[10] RNA sequencing (RNA-seq) confirmed that, similar to human ASCL1-positive SCLCs, *RPR2* GEMM tumors repressed antigen-presentation genes (Figures S1A and S1B). Moreover, cell lines derived from *RPR2* GEMMs repressed surface MHC-I, and MHC-I was partially restored by treatment with interferon γ (IFNγ) (Figure S1C), as shown previously,[10,11] supporting a non-genetic mechanism of MHC-I repression. After lung tumors developed as determined by lung MRI, we performed a pharmacodynamic (PD) study to test whether LSN3321213 effectively blocked Aurora A kinase activity in lung tumors. Tumors treated with LSN3321213 had increased serine 10 phosphorylation on histone H3 (H3S10P) consistent with AURKA being blocked by LSN3321213 (Figure 1B). Selectivity of LSN3321213 for AURKA over AURKB was confirmed in four different mouse SCLC cell lines (Figures S2A and S2B). We next performed an efficacy study with LSN3321213 alone or when combined with a PD-L1 antibody. SCLC autochthonous lung tumors were initiated as above and lung tumors were confirmed with lung MRI. Mice with tumors were then randomized into four treatment arms: (1) vehicle, (2) PD-L1 alone, (3) LSN3321213 alone, or (4) combination of LSN3321213 and PD-L1 administered concurrently. Initial tumor volumes at enrollment were similar among all treatment arms (Figure 1C). Lung

Figure 1. The Aurora A kinase inhibitor LSN3321213 combined with PD-L1 immune checkpoint blockade is efficacious in an autochthonous immunocompetent genetically engineered mouse model of small cell lung cancer

(A) Schematic of the autochthonous CRISPR-based genetically engineered mouse model (GEMM) of small cell lung cancer (SCLC) used for the studies in Figures 1, 3, 4, 5, and 6. *RPR2* = sg*Rb1*, sg*Trp53*, and sg*Rbl2*. sgC0111, non-targeting sgRNA.

(B) Immunoblot analysis of SCLC tumors isolated from SCLC GEMM in (A) treated with the Aurora A kinase inhibitor (AURKAi) LSN3321213 at 57 mg/kg by mouth (p.o.) twice a day (BID) or vehicle (H_3PO_4) for 3.5 days (7 doses).

(C) Initial tumor volumes before the treatment indicated determined by lung MRI.

(D) Treatment schematic for the efficacy studies in Figure 1 using the autochthonous SCLC GEMM.

(E) Lung MRI of representative LSL-Cas9 mice with lung tumors at baseline and after 14 days and 28 days of treatment with vehicle (H_3PO_4), PD-L1 (200 μg/mouse 3×/week), LSN3321213 (57 mg/kg p.o. BID), or combined LSN3321213 (57 mg/kg p.o. BID) and PD-L1 (200 μg/mouse 3×/week). Red pseudo-coloring denotes tumors. Scale bar, 1 cm.

(F and G) Tumor volumes of lung tumors from mice in (C) on day 14 determined by lung MRI after the indicated treatment relative to tumor volumes at baseline represented as a bar graph (F) or waterfall plot (G). n = 8 mice (vehicle), n = 7 mice (PD-L1), n = 8 mice (LSN3321213), n = 10 mice (LSN3321213 + PD-L1).

(H and I) Tumor volumes of lung tumors on day 28 determined by lung MRI of the mice that remained alive after the treatments indicated relative to tumor volumes at baseline represented as a bar graph (H) or waterfall plot (I). n = 7 mice (vehicle), n = 3 mice (PD-L1), n = 5 mice (LSN3321213), n = 9 mice (LSN3321213 + PD-L1). For (G) and (I), X indicates mice enrolled in the study that were no longer alive at the time MRI were performed.

(J) Kaplan-Meier survival of mice with lung tumors treated with vehicle, PD-L1, LSN3321213, or combined LSN3321213 and PD-L1. n = 8 mice (vehicle), n = 7 mice (PD-L1), n = 8 mice (LSN3321213), n = 10 mice (LSN3321213 + PD-L1). *$p < 0.05$, **$p < 0.01$. Data are represented as mean ± SEM in (C), (F), and (H). See also Figures S1–S4 and Table S1.

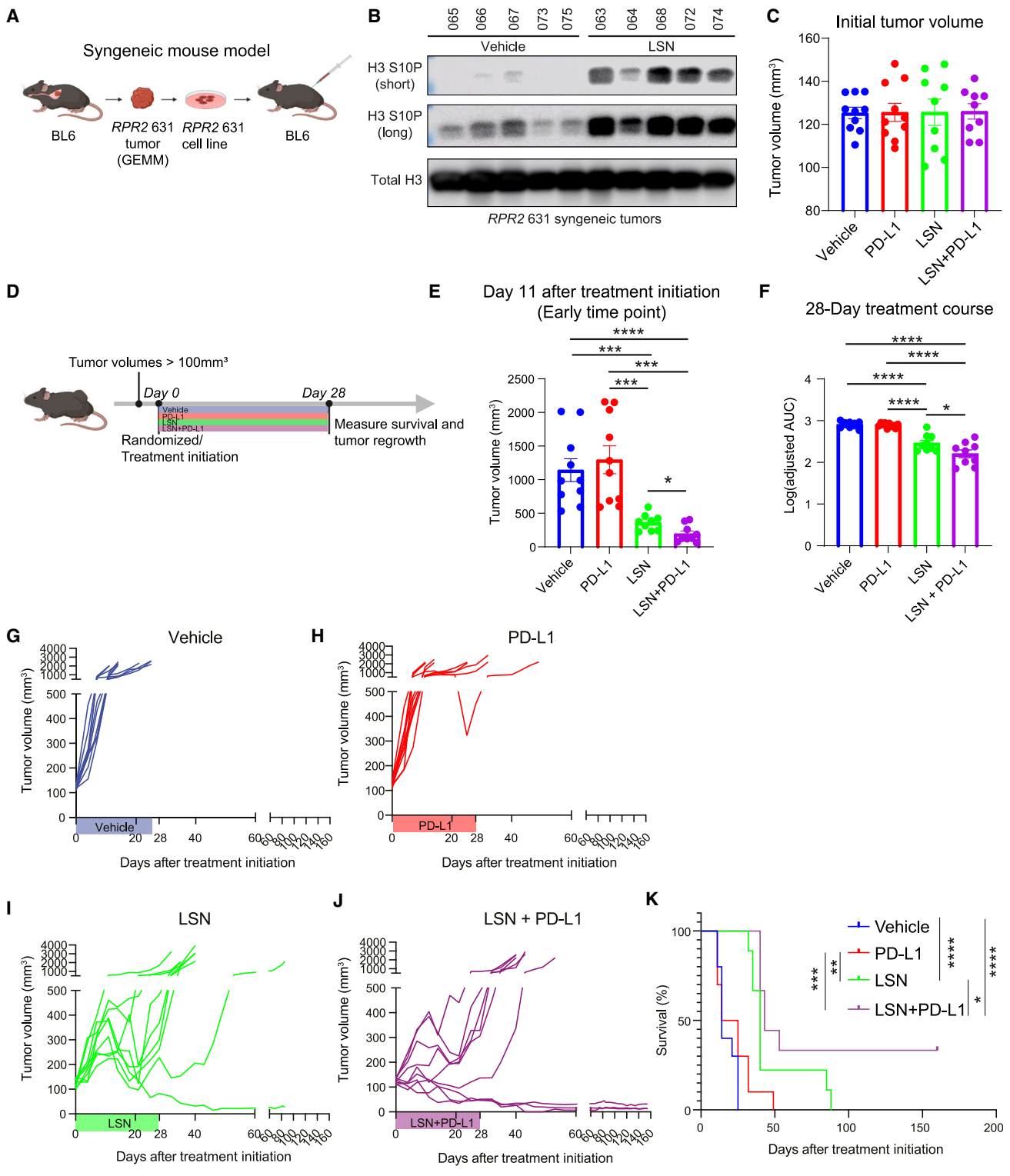

Figure 2. The Aurora A kinase inhibitor LSN3321213 combined with PD-L1 is efficacious and induces some complete responses in a syngeneic immunocompetent mouse model of SCLC

(A) Schematic of the *RPR2* 631 syngeneic immunocompetent mouse model of SCLC. *RPR2* = sg*Rb1*, sg*Trp53*, and sg*Rbl2*.

(B) Immunoblot analysis of SCLC tumors isolated from the *RPR2* 631 syngeneic model in (A) treated with the AURKAi LSN3321213 at 57 mg/kg p.o. BID or vehicle (H_3PO_4) for 3.5 days (7 doses).

(legend continued on next page)

MRI was performed at 2 and 4 weeks after treatment initiation to monitor response, and subsequently mice were monitored for survival (see Figure 1D for treatment schema; also see STAR Methods). Lung MRI after 2 weeks of treatment showed a significant reduction in lung tumor growth in mice treated with LSN3321213 or combined LSN3321213 and PD-L1, but not with PD-L1 alone, all compared to mice treated with vehicle (Figures 1E–1G; Table S1A); 70% of tumors (seven of 10) in mice treated with combined LSN3321213 and PD-L1 decreased in size (Figure 1G; Table S1A). At the 2-week early time point, there was no statistical significance between mice treated with combined LSN3321213 and PD-L1 compared to mice treated with LSN3321213 alone, suggesting that the initial response was primarily driven by AURKAi in tumors (Figure 1F; Table S1B). After 4 weeks of treatment, tumor volumes from mice treated with combined LSN3321213 and PD-L1 were significantly reduced compared to mice treated with vehicle or PD-L1 alone, while tumors from mice treated with LSN3321213 alone were not significantly smaller compared to vehicle or PD-L1 alone (Figures 1E, 1H, and 1I; Tables S1C and S1D). Although there was a trend toward increased anti-tumor efficacy at the late time point with combined LSN3321213 and PD-L1 compared to LSN3321213 alone, the data did not reach statistical significance ($p = 0.07$, relative risk [RR] = 0.32, 95% CI [0.09, 0.94]) (Table S1D). Median survival was significantly increased with the combination of LSN3321213 and PD-L1 compared to vehicle ($p = 0.01$) or PD-L1 alone ($p = 0.02$), while there was no increase in survival with LSN3321213 alone compared to vehicle or PD-L1 alone (Figure 1J).

Upon necropsy, nearly all mice had lung tumors that were histologically consistent with SCLC and most mice had liver metastases (Figure S3A). LSN3321213 alone or the combination of LSN3321213 and PD-L1 was tolerated as there were no significant differences in body weights in any of the treatment groups over the 28 days of treatment (Figure S4A) nor were there any differences in white blood cell counts or hematocrits among the treatment groups (Figures S4B and S4C). The efficacy of the combination of LSN3321213 and PD-L1 ICB was not simply a consequence of the PD-L1 antibody increasing plasma drug concentrations of LSN3321213 as mice that received LSN3321213 alone or LSN3321213 and PD-L1 had similar LSN3321213 plasma concentrations (Figure S4D). Together, these data show that LSN3321213 has anti-tumor activity in this model, but its activity is short lived, whereas the combination of LSN3321213 + PD-L1 induces a more durable anti-tumor response leading to a significant increase in survival.

Combination treatment with the Aurora A kinase inhibitor LSN3321213 and PD-L1 has activity in a syngeneic small cell lung cancer immunocompetent mouse model

We next asked whether LSN3321213 or LSN3321213 + PD-L1 had efficacy in a syngeneic immunocompetent SCLC mouse model.[10,24] This model was developed by isolating an SCLC cell line (originally called *RPP* 631, now called *RPR2* 631 to be consistent with gene nomenclature) from an autochthonous SCLC lung tumor generated from our CRISPR-based SCLC GEMM where *Rb1*, *Trp53*, and *Rbl2* were inactivated in a pure BL6 mouse. We subcutaneously injected *RPR2* 631 cells back into BL6 mice and allowed tumors to form (Figure 2A). Once tumors were ~100 mm^3, a PD study was performed by treating tumor-bearing mice with six doses of LSN3321213 or vehicle (see STAR Methods), which showed that LSN3321213 increased H3S10P consistent with inhibition of Aurora A kinase activity in tumors (Figure 2B). *RPR2* 631 cells were then again subcutaneously injected into BL6 mice. Once tumors were ~100 mm^3 (Figure 2C), mice were randomized to four groups that either received (1) vehicle, (2) PD-L1, (3) LSN3321213, or (4) combination of LSN3321213 and PD-L1 and were treated for 28 days. Mice were then monitored off treatment for survival (see Figure 2D for treatment schema). Tumor volumes were measured with calipers at multiple time points. In this model, treatment with either LSN3321213 or combined LSN3321213 and PD-L1 had significant activity, each reducing tumor growth compared to vehicle at all time points throughout the study (Figures 2E–2J; Tables S2A and S2B). PD-L1 had no significant effect on tumor growth, which is consistent with a previous study with PD-1 ICB using the *RPR2* 631 model[24] (Figures 2E, 2F, and 2H). Either treatment with LSN3321213 alone or combined LSN3321213 and PD-L1 significantly increased survival compared to vehicle or PD-L1 (Figure 2K). Combined LSN3321213 and PD-L1 more potently inhibited tumor growth compared to LSN3321213 alone throughout the 28-day treatment course (Figure 2F; Tables S2C and S2D). Notably, three of 10 mice treated with LSN3321213 + PD-L1 and one out of 10 mice treated with LSN3321213 had a near-complete response resulting in long-term remissions without evidence of tumor re-growth (Figures 2I and 2J). Combined LSN3321213 + PD-L1 increased overall survival compared to LSN3321213 alone (Figure 2K). Of note, after 2 weeks of treatment, two mice treated with LSN3321213 alone and one mouse treated with LSN3321213 + PD-L1 lost weight. At that point, LSN3321213 was held for 1 day and then restarted at half the dose, which was well tolerated thereafter (Figure S4E). These results show that either LSN3321213 or combined LSN3321213 +

(C) Initial tumor volumes before the treatments indicated determined using calipers.
(D) Treatment schematic for the efficacy studies using the syngeneic SCLC *RPR2* 631 xenograft model.
(E) Tumor volumes on day 11 (the last day that all mice remained alive in all treatment groups) after indicated treatment determined using calipers.
(F) Log-transformed adjusted AUCs (see STAR Methods) of tumor volumes for the indicated treatments using all time points throughout the 28-day full treatment course.
(G–J) Spider plots of individual *RPR2* 631 xenograft tumors treated with vehicle (H_3PO_4) (G), PD-L1 (200 μg/mouse 3×/week) (H), LSN3321213 (57 mg/kg p.o. BID) (I), or combined LSN3321213 (57 mg/kg p.o. BID) and PD-L1 (200 μg/mouse 3×/week) (J) for 28 days. Note: all vehicle mice reached their endpoint in tumor volume by 25 days. n = 10 mice (vehicle), n = 10 mice (PD-L1), n = 9 mice (LSN3321213), n = 9 mice (LSN3321213 + PD-L1). Colored box on x axis indicates treatment duration.
(K) Kaplan-Meier survival of mice with *RPR2* 631 xenografts treated with vehicle, PD-L1, LSN3321213, or combined LSN3321213 and PD-L1. For (C)–(I), n = 10 mice (vehicle), n = 10 mice (PD-L1), n = 9 mice (LSN3321213), n = 9 mice (LSN3321213 + PD-L1). *$p < 0.05$, **$p < 0.01$, ***$p < 0.001$, ****$p < 0.0001$. Data are represented as mean ± SEM in (C), (E), and (F). See also Figure S4 and Table S2.

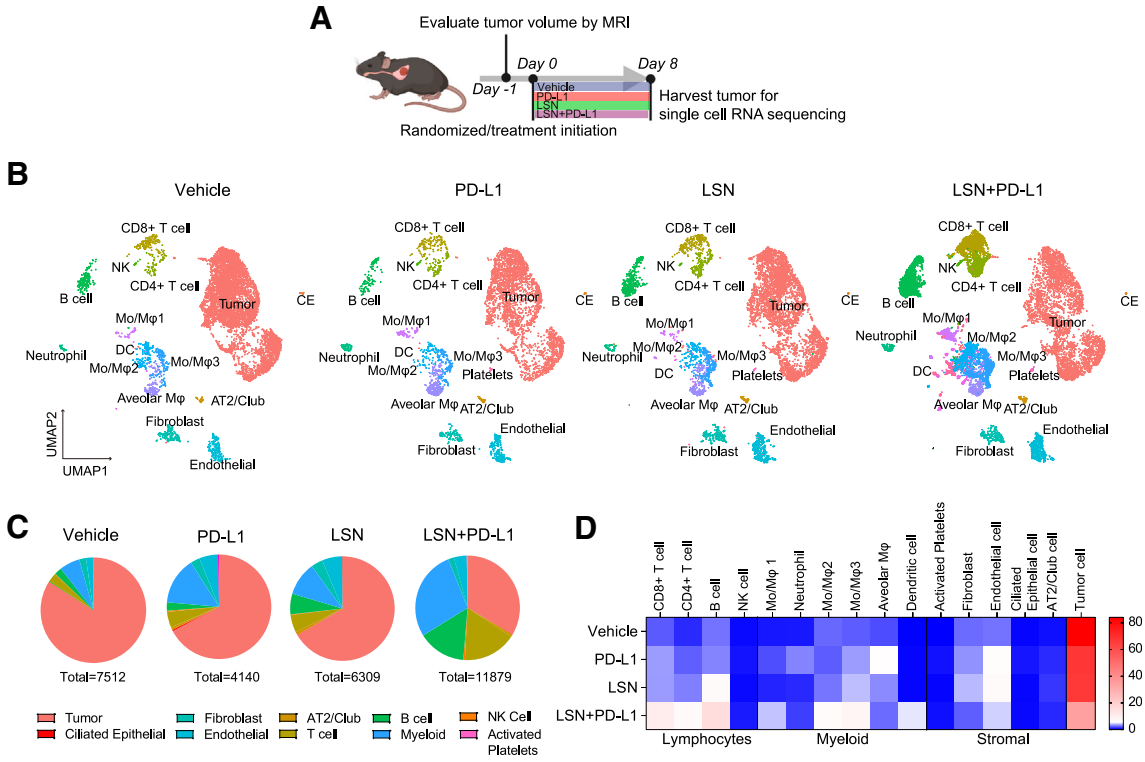

Figure 3. The Aurora A kinase inhibitor LSN3321213 combined with PD-L1 increases immune cells in autochthonous SCLC tumors

(A) Schematic for the single-cell RNA-seq experiments performed on autochthonous SCLC tumors from our CRISPR-based GEMM (see Figure 1A and STAR Methods) after 8 days of treatment with vehicle (H_3PO_4), PD-L1 (200 μg/mouse 3×/week), LSN3321213 (57 mg/kg p.o. BID), or combined LSN3321213 (57 mg/kg p.o. BID) and PD-L1 (200 μg/mouse 3×/week).

(B) Uniform Manifold Approximation and Projection (UMAP) after integration of all cells from nine tumors each from independent mice. n = 7,512 cells from two tumors from independent mice (vehicle), n = 4,140 cells from two tumors from independent mice (PD-L1), n = 6,309 cells from two tumors from independent mice (LSN3321213), and n = 11,879 cells from three tumors from independent mice (LSN3321213 + PD-L1). Cell types were confirmed based on the expression level of representative markers (see Figure S5). CE, ciliated epithelial cell; DC, dendritic cell; Mo/Mφ, monocytes/macrophages.

(C) Pie charts representing the percentages of major cell types in (B) in the different treatment conditions indicated.

(D) A heatmap of the percentage of each cell type relative to the total cell number from each treatment group using data from (B). See also Figures S5, S6, and Table S3.

PD-L1 have anti-tumor efficacy in the *RPR2* 631 SCLC mouse model. The combination of LSN3321213 + PD-L1 caused a more significant reduction in tumor growth leading to a significant increase in survival compared to LSN3321213 alone.

Combined Aurora A kinase inhibition and PD-L1 treatment increases T lymphocyte infiltration in SCLC tumors

We next sought to understand how AURKAi and PD-L1 exert a combinatorial anti-tumor effect. Expression of genes involved in antigen presentation and innate immune signaling significantly correlates with response to immunotherapy in human SCLC.[10,13,14] Thus, we hypothesized that LSN3321213 increased innate immune signaling in tumor cells, thereby "priming" tumors for an improved PD-L1 response. To test this, we performed single-cell RNA-seq (scRNA-seq) in autochthonous SCLC lung tumors from an additional cohort of tumor-bearing mice treated with (1) vehicle, (2) PD-L1, (3) LSN3321213, or (4) LSN3321213 and PD-L1 for 1 week (Figures 3A and S3B). UMAP clustering of all cells sequenced showed a striking enrichment in several immune cell subsets, including $CD8^+$ T cells, $CD4^+$ T cells, B cells, and macrophages with a relatively depleted fraction of tumor cells after LSN3321213 and PD-L1 treatment, whereas LSN3321213 or PD-L1 alone more modestly increased the immune cell fraction within tumors (Figures 3B–3D, S5A–S5C, and S6A). Consistent with samples from SCLC patients, tumor cells largely did not express PD-L1, but PD-L1 was expressed on several immune cell types with a modest increase in its expression on immune cells in tumors treated with LSN3321213 and PD-L1 (Figure S6B). PD-1 was primarily expressed on T lymphocytes and its expression was robustly increased after combined LSN3321213 and PD-L1 treatment (Figure S6C). These results show dynamic increases in immune cells within tumors after combined treatment with LSN3321213 and PD-L1, and, together with our efficacy data (see Figures 1 and 2), suggest a role for blocking the PD-L1/PD-1 inhibitory checkpoint following LSN3321213 treatment to achieve a more robust and durable anti-tumor immune response.

Given the increase in T cells in tumors treated with LSN3321213 and PD-L1 vs. vehicle and the impact that T cells have on anti-tumor immune responses,[26–29] we further characterized the T cell and natural killer (NK) cell populations in tumors under different treatment conditions. UMAP clustering of cells in $CD3^+$ T cell and

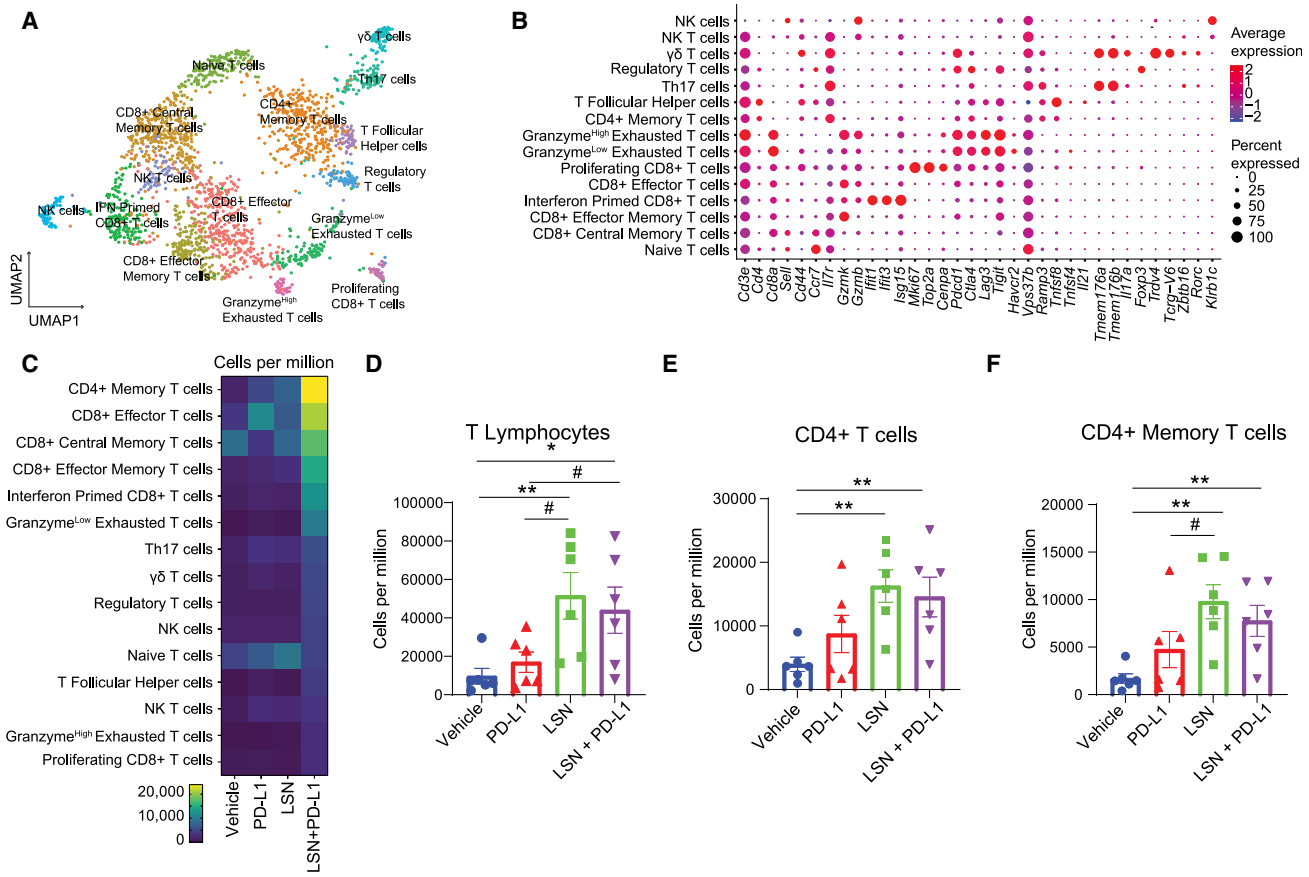

Figure 4. Analysis of T lymphocytes in murine SCLC tumors

(A) UMAP projections of single T lymphocytes and NK cells from all nine tumors showing the composition of different lymphocyte subpopulations in autochthonous SCLC tumors.

(B) Dot plot showing the average expression of marker genes to identify immune cell subpopulations of all cells in (A). The size of the dot represents the percentage of cells expressing a particular gene, while color represents the mean gene expression levels (blue is low and red is high).

(C) A heatmap of the number of cells from the indicated cell type per million total cells from (A) in the treatment groups indicated (dark blue is low and green is high).

(D–F) Quantitation of flow cytometry analysis of T lymphocyte subpopulations displayed as cells per million within tumors after 1 week of treatment with vehicle (H_3PO_4), PD-L1 (200 μg/mouse 3×/week), LSN3321213 (57 mg/kg p.o. BID), or combined LSN3321213 (57 mg/kg p.o. BID) and PD-L1 (200 μg/mouse 3×/week). (D) Total T lymphocytes identified by CD45+/CD19−/CD3+/CD49b−, (E) = CD4+ T cells ($CD4^+$), F=CD4+ memory T cells (CD4+/CD44+). For (D)–(F), n = 6 tumors from independent mice for each treatment group. #$p < 0.1$, *$p < 0.05$, **$p < 0.01$, ***$p < 0.001$. Data are represented as mean ± SEM in (D)–(F). See also Figures S7, S8, and Table S3.

NK cell clusters identified multiple T cell subsets within the tumor microenvironment (Figures 4A and 4B). Tumors from mice treated with LSN3321213 and PD-L1 were most highly enriched with $CD4^+$ memory T cells (*Cd3e+/Cd4+/Cd44+*), $CD8^+$ effector T cells (*Cd3e+/Cd8a+/Sell−/Cd44+/Gzmk* and/or *Gzmb+*), $CD8^+$ central memory (*Cd3e+/Cd8a+/Sell+/Cd44+*), $CD8^+$ effector memory T cells (*Cd3e+/Cd8a+/Sell−/Cd44+*), and interferon-primed $CD8^+$ T cells (*Cd3e+/Cd8a+/Gzmk* and/or *Gzmb+/Ifit1*, *Ifit3*, and *Isg15+*) compared to all other treatment arms without robust changes in naive T cells (Figure 4C; Table S3A) consistent with a productive anti-tumor T cell immune response.[30,31]

To determine whether increased lymphocyte infiltration is robust across SCLC models, we used our *RPR2* 631 syngeneic model to characterize immune cell subsets by flow cytometry after treatment of tumor-bearing mice with (1) vehicle, (2) PD-L1, (3) LSN3321213, or (4) LSN3321213 and PD-L1 for 1 week (Figure S7A). PD-L1 fluorescence-activated cell sorting (FACS) analysis showed significant decreases in PD-L1 surface expression on immune cells, demonstrating that the PD-L1 antibody effectively blocked PD-L1 in tumors (Figures S7B and S7C). Consistent with our scRNA-seq data from the autochthonous CRISPR-based SCLC GEMM, flow cytometry showed a significant increase in $CD3^+$ T cells in tumors treated with combined LSN3321213 and PD-L1 or LSN3321213 alone compared to vehicle (Figure 4D; Table S3B). Tumors treated with combined LSN3321213 and PD-L1 or LSN3321213 alone had a significant increase in intra-tumoral $CD4^+$ T cells and a trend toward significance of intra-tumoral $CD8^+$ T cells (Figures 4E and S7D). Furthermore, there was a significant increase in intra-tumoral memory $CD4^+$ T cells after treatment with LSN3321213 and PD-L1 or LSN3321213 alone, and a significant increase in central memory $CD8^+$ T cells after treatment with LSN3321213 and PD-L1, all compared to vehicle (Figures 4F

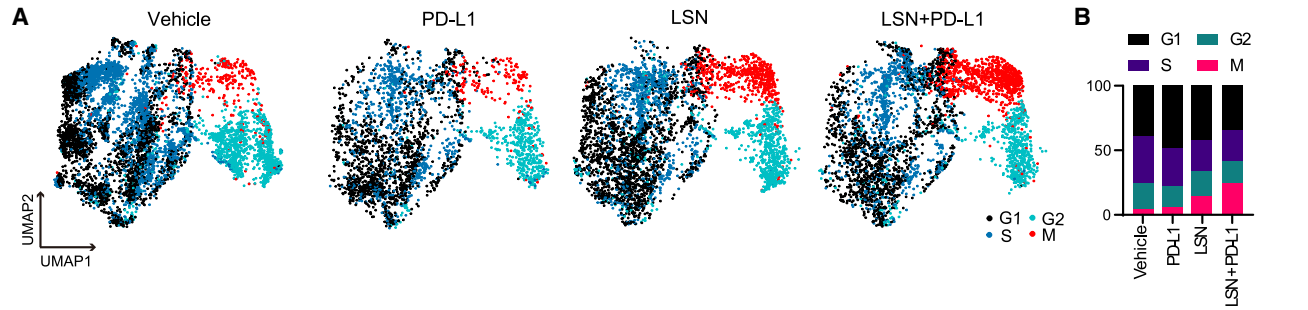

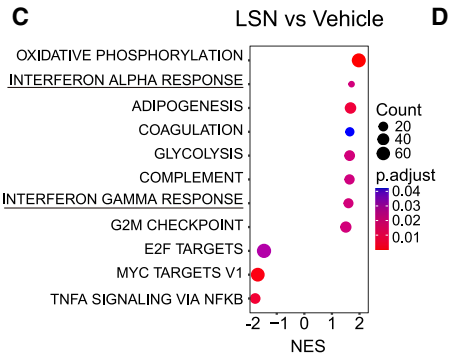

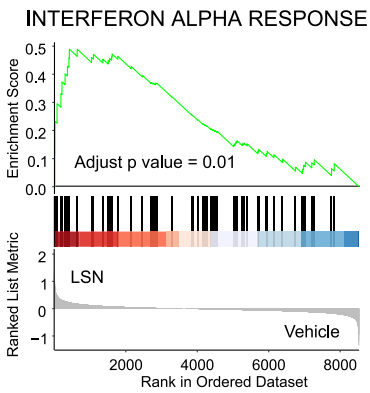

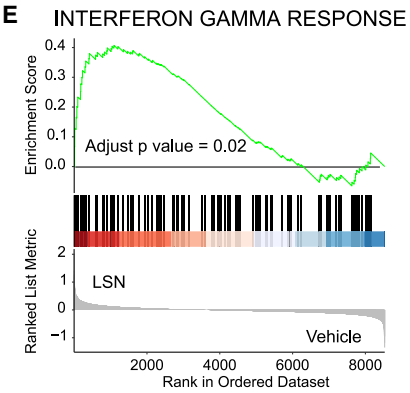

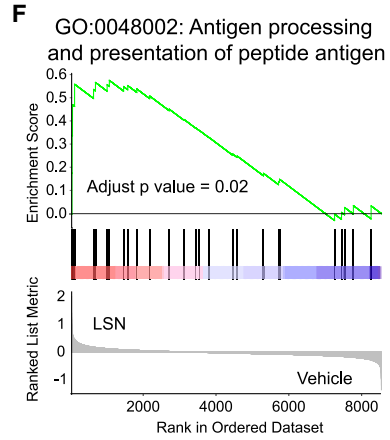

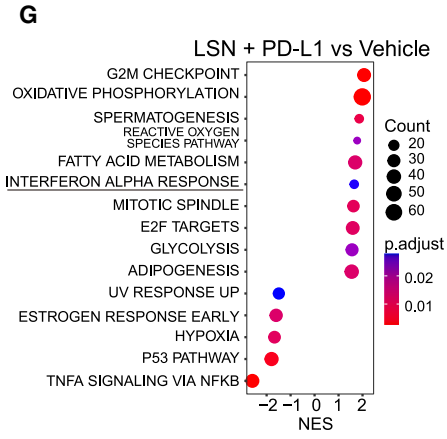

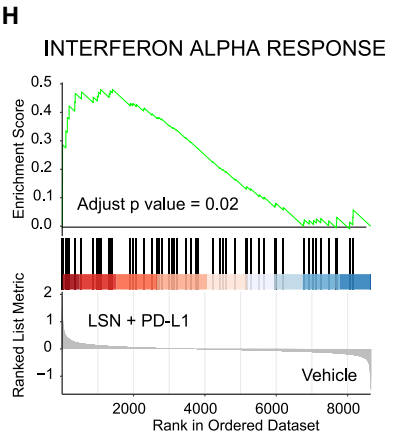

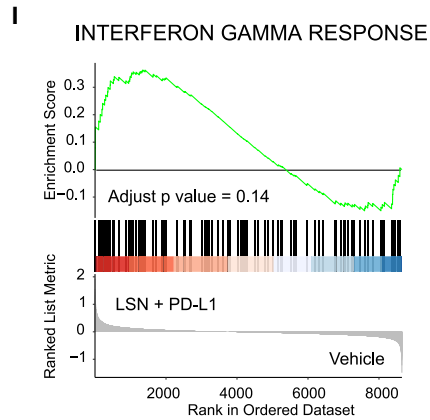

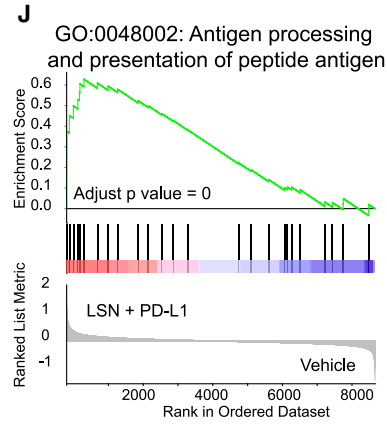

(legend on next page)

and S7E–S7I). One difference between our scRNA-seq data in autochthonous SCLC GEMMs and our FACS analysis in syngeneic subcutaneous SCLC xenografts was that LSN3321213 treatment alone was sufficient to induce a robust infiltration of lymphocytes within subcutaneous xenograft tumors and there were no additional infiltrated lymphocytes when LSN3321213 was combined with PD-L1. These differences could be related to differences in the tumor immune microenvironment or vasculature of a subcutaneous xenograft model compared to the native lung tumor microenvironment.[32–35] We also analyzed whether there were changes in myeloid cell infiltration within tumors after LSN3321213 or LSN3321213 + PD-L1 treatment. Consistent with a previous study in a breast cancer syngeneic model 4T1 treated with alisertib,[36] our scRNA-seq data and FACS analysis showed that CD11c-positive tumor-associated macrophages (TAMs) were decreased after LSN3321213 or LSN3321213 + PD-L1 treatment in our scRNA-seq and FACS data (Figures S8A–S8D). Together, these data show that AURKAi increases lymphocyte infiltration within SCLC tumors and lymphocyte infiltration is further increased when AURKAi is combined with PD-L1 in autochthonous SCLC GEMMs.

Aurora A kinase inhibition augments innate immune signaling in tumor cells

To better understand why tumors treated with LSN3321213 and PD-L1 had increased immune cell infiltration, we further analyzed our scRNA-seq data. We performed UMAP analysis on tumor cells selected by *GFP*-positive and *Cas9*-positive clustering as our SCLC GEMM is derived from LSL-Cas9-P2A-GFP mice and therefore tumor cells are Cas9 and GFP positive (see STAR Methods and Figure S7C). We then identified tumor cells in different phases of the cell cycle. Consistent with the known consequences of AURKAi arresting cells in mitosis,[37,38] tumors treated with LSN3321213 and PD-L1 or LSN3321213 alone had a statistically significant increased fraction of tumor cells in M phase compared to vehicle (Figures 5A, 5B, and S9A–S9G). Interestingly, lymphocytes (T cells, NK cells, and B cells) within tumors did not have an increased proportion of G2/M cells after treatment with LSN3321213 (or LSN3321213 and PD-L1); while similar to tumor cells, the G2/M proportion of myeloid cells was increased after LSN3321213 (or LSN3321213 and PD-L1) (Figures S10A–S10F). Together, this demonstrates that tumor cells and myeloid cells are more sensitive to AURKAi, whereas lymphocytes are more resistant. This also suggests a therapeutic window allowing for AURKAi in tumor cells while preserving the ability of T cells and NK cells to proliferative in the presence of LSN3321213 to induce an anti-tumor immune response.

We then calculated differentially expressed genes (Table S4) and performed gene set enrichment analysis (GSEA) on all tumor cells comparing LSN3321213 and PD-L1 or LSN3321213 alone to vehicle. Consistent with AURKAi blocking cells in M phase, GSEA showed that LSN3321213 and PD-L1 or LSN3321213 alone had significant enrichment of the G2M checkpoint and mitotic spindle gene sets (Figures 5C and 5F). Interestingly, we also found significant enrichment of interferon α and γ response genes and antigen-presentation genes in LSN3321213 and PD-L1 or LSN3321213 treated tumor cells (Figures 5C–5J). Similarly, bulk RNA-seq from independent autochthonous SCLC tumors treated with LSN3321213 or vehicle from our PD experiment (see Figure 1B) also showed significant enrichment of interferon response genes (Figures S11A–S11C; Table S5). Together, these data suggest increased interferon signaling in tumor cells after LSN3321213 treatment.

Using our scRNA-seq data, we then interrogated tumor cell/immune cell interactions that could lead to a productive anti-tumor immune response. To do this, cell-cell interaction analysis[39] was performed to first identify differential ligand expression on immune/stromal cells in LSN3321213 and PD-L1 compared to vehicle and then identify enriched gene expression in tumor cells that corresponded with enrichment of the ligand on immune cells. The results show an enrichment of several ligands on various immune cells in tumors treated with LSN3321213 and PD-L1 compared to vehicle (Figure 6A, left). Several of these ligands on immune cells have been previously linked to productive anti-tumor immune responses, including *Gzmb* (granzyme b),[40] *Cxcl9*,[41,42] *Cxcl10*,[41,42] *Ifng* (interferon γ),[43] and *Penk*[44] (Figure 6A). The corresponding enrichment of expression to this set of ligands in the tumor cells converged on genes stimulated by IFNγ or TNFα (Figure 6A, right) with enrichment of IFNγ-stimulated genes in tumor cells correlating with enhanced immunogenicity in SCLC.[10] Consistent with this, UMAP analysis found enrichment of *Ifng* expression selectively on *CD4*$^+$ and *CD8*$^+$ T cells and increased expression of interferon-stimulated genes in tumor cells treated with LSN3321213 and PD-L1 (or more modestly with LSN3321213 alone) compared to vehicle (Figure 6B). Of note, tumor cell IFNγ receptor expression is not grossly altered by LSN3321213 and/or PD-L1 treatment suggesting that expression changes in interferon target genes were not simply a consequence of increased IFNγ receptors on tumor cells (Figures S12A–S12D).

One of the interferon response genes most highly upregulated in tumor cells after LSN3321213 and PD-L1 treatment was *B2m* (Figure 6A), which is (1) required for MHC-I antigen presentation; (2) silenced, along with MHC-I surface expression in most SCLCs; and (3) B2M loss is a conserved mechanism of

Figure 5. The Aurora A kinase inhibitor LSN3321213 blocks cells in M phase unmasking a cell state with high interferon signaling

(A) UMAP projections of single cells from tumor clusters from Figure 3B showing different phases of the cell cycle in each treatment group indicated. Cell cycle phases were determined based on the expression level of representative markers (see Figure S10).

(B) Quantitation of phases of the cell cycle from (A) depicted in stacked bar graphs showing the percentage of each cell cycle phase in each treatment group.

(C–J) Dot plot representations of gene set enrichment analysis (GSEA) (C and G) ranked by normalized enrichment scores (NESs) for LSN vs. vehicle (C) and LSN + PD-L1 vs. vehicle (G) using Hallmark pathway gene sets showing significantly enriched and depleted pathways for each treatment comparison indicated. The size of the dot represents the number of genes belonging to a particular signature while color represents the Benjamini-Hochberg adjusted p value (cutoff = 0.05); red is low and blue is high. Enrichment plots of the interferon α (D and H) and γ gene sets (E and I) using Hallmark pathway gene sets, and the antigen processing and presentation of peptide antigen gene set (F and J). See also Figures S9–S11 and Tables S4–S7.

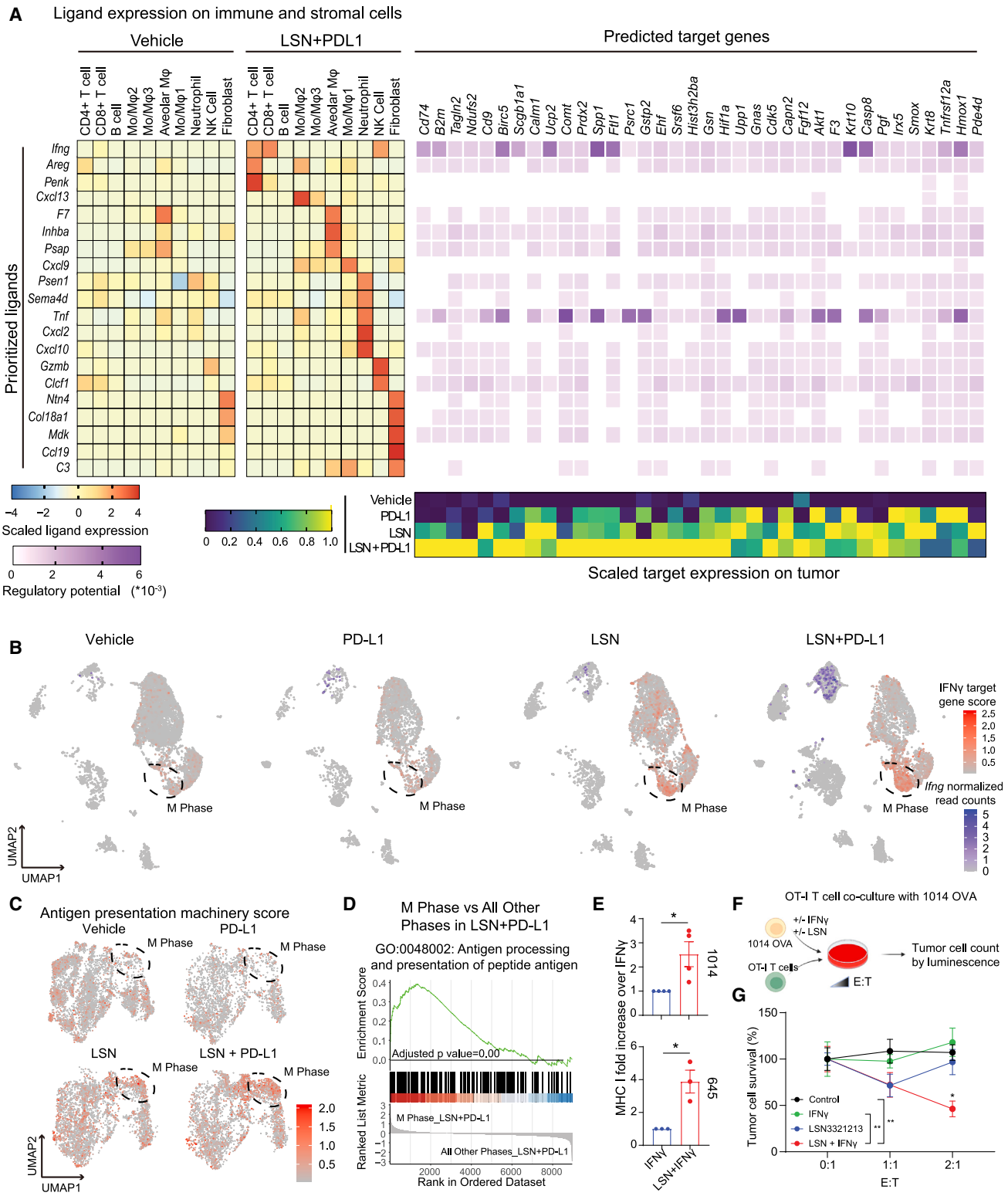

Figure 6. LSN3321213 + PD-L1 induces IFNγ production in T lymphocytes, which correlates with increased IFNγ target genes in M phase tumor cells

(A) Differential NicheNet tumor and its microenvironment communication analysis (see STAR Methods) using scRNA-seq from Figure 3B comparing combined LSN3321213 and PD-L1 vs. vehicle. Left: a heatmap of top 20 differentially expressed ligands on immune and stromal cell populations (based on prioritization

(legend continued on next page)

immunotherapy resistance across several cancer types.[8,45,46] SCLCs with restored MHC-I surface expression have more durable responses to ICB and are more non-neuroendocrine with higher TAP1 and AXL and lower ASCL1 expression.[10,14] Consistent with this, *B2M* expression significantly correlated with *TAP1* and *AXL* in human SCLC tumors (Figures S13A and S13B). Interestingly, increased expression of IFNγ-stimulated genes and antigen-presentation genes, including *B2m*, occurred in tumor cells that were in M phase of the cell cycle after treatment with LSN3321213 and PD-L1 (Figures 6B–6D and S14A–S14G). Also, ASCL1 and ASCL1 target genes were significantly depleted when comparing M phase vs. all other cell cycle phases in tumors treated with LSN3321213 + PD-L1 and also when comparing all tumor cells treated with LSN3321213 + PD-L1 vs. vehicle (Figures S15A and S15B), supporting the opposing relationship between SCLC tumor immunogenicity and ASCL1 neuroendocrine differentiation.[10,14] Enrichment of antigen-presentation genes and depletion of ASCL1 target genes was also observed in M phase vs. all other cell cycle phases in vehicle-treated tumors (Figures S15C and S15D), showing that antigen presentation is relatively enriched and ASCL1 is relatively depleted in mitosis. Clearly, genes driving antigen presentation (e.g., *B2m*, *Cd74*) or *Ascl1* (e.g., *Ascl1*, *Nfib*) were some of the top upregulated and downregulated genes, respectively, in all tumor cells after treatment with LSN3321213 and PD-L1 compared to vehicle (Figure S15B; Table S4). Together, these data suggest that enhanced expression of interferon and antigen-presentation genes is due to AURKAi enriching the fraction of cells in mitosis.

Consistent with our *in vivo* results, LSN3321213 significantly augmented *B2m* mRNA expression and MHC-I surface expression in response to IFNγ in tumor cell lines (1014 and 645) derived from our CRISPR-based GEMM (Figures 6E and S16A–S16D), and cell surface MHC-I expression required TAP1 (Figures S16E and S16F). Similarly, LSN3321213 + IFNγ significantly increased MHC-I compared to IFNγ alone in two different human ASCL1-positive SCLC cell lines (Figures S17A–S17D). Like LSN3321213, *AURKA* CRISPR inactivation with two independent sgRNAs in mouse 1014 cells also enhanced IFNγ-induced MHC-I expression, suggesting that LSN3321213 MHC-I induction is likely on-target (Figures S18A–S18C). Moreover, increased tumor cell MHC-I by LSN3321213 + IFNγ sensitized tumor cells to T cell cytotoxicity in co-culture experiments where 1014 cells transduced with exogenous ovalbumin (OVA) were mixed with OT-1 Cd8a+ T cells[10] (see STAR Methods) (Figures 6F, 6G, and S19A). Consistent with our scRNA-seq data, primary OT-1 Cd8a+ T cells were resistant to LSN3321213 (Figure S19B). Together, these data show that AURKAi in the presence of IFNγ increases MHC-I expression on SCLC cells, which can promote antigen-specific killing by $CD8^+$ T cells.

To determine whether other mitotic inhibitors similarly increase antigen presentation and decrease ASCL1, we tested other mitotic inhibitors, including another AURKAi (MK-5108), an AURKBi (AZD2811), and paclitaxel at concentrations slightly above their half-maximal effective concentration (EC_{50}) (Figures S20A and S20B). Similar to LSN3321213, MK-5108, AZD2811, and paclitaxel, when combined with IFNγ, also increased MHC-I compared to IFNγ alone, although MHC-I expression was most consistently increased by the AURKAi LSN3321213 and MK-5108 (Figures S20C and S20D). LSN3321213, MK-5108, and paclitaxel also decreased ASCL1 protein levels in both mouse and human SCLC cell lines (Figure S20E). Together, these results demonstrate that AURKAi, as well as other mitotic inhibitors, increase MHC-I and decrease ASCL1 expression in mouse and human SCLCs of the ASCL1 subtype.

Last, we asked whether the combination of LSN3321213 + PD-L1 elicits protective immunity in mice. We performed an additional *in vivo* syngeneic experiment in BL6J mice using mouse 1014 P2 cells; another SCLC cell line isolated from our CRISPR-based *RPR2* GEMM (see STAR Methods). Once tumors developed (~100 mm^3), mice were randomized 3:1 to the combination of LSN3321213 + PD-L1 or vehicle for 28 days. Consistent with our results in the *RPR2* 631 syngeneic model (Figure 2), LSN3321213 + PD-L1 potently inhibited tumor growth in the 1014 P2 syngeneic model with seven out of 18 mice having a complete response and no evidence of recurrence 5 weeks following the 28-day treatment period (Figures 7A–7D, S21A, and S21B). At this time (5 weeks after completion of treatment), these complete responders and age-matched "naive" control BL6J were reinjected with the same 1014 P2 cells. Strikingly, tumors did not grow in any of the rechallenged mice but grew in all of the naive mice (Figure 7E), demonstrating that treatment with LSN3321213 + PD-L1 promotes immunological memory, allowing mice to reject a subsequent subcutaneous transplant.

score; see STAR Methods) in LSN3321213 and PD-L1 vs. vehicle (blue = low and red = high). Right: a heatmap of differentially expressed genes after LSN3321213 and PD-L1 vs. vehicle in tumor cells that are also predicted target genes of ligands identified on immune/stromal cells (left). Their potential to be regulated by the ligands in immune/stromal cells is depicted by the heatmap where white is low and purple is high. Bottom right: a heatmap of scaled predicted target gene expression (top) on tumor cells from the treatments indicated (navy = low and green = high).

(B) UMAP projections of cells according to treatment showing immune and stromal cell *Ifng* expression (gray = low and blue = high) and tumor cell IFNγ target gene scores (gray = low and red = high) with M phase cells indicated.

(C) UMAP projections of tumor cells according to treatment showing antigen-presentation gene score (gray = low and red = high) with M phase cells indicated.

(D) Enrichment plots of the antigen processing and presentation of peptide antigen gene set showing significant enrichment of antigen-presentation genes in M phase within LSN + PD-L1-treated tumors.

(E) Quantification of cell surface MHC-I protein expression by flow cytometry of 1014 and 645 cells treated with LSN3321213 (125 nM) or LSN3321213 (125 nM) and IFNγ (10 ng/mL). For 1014, n = 4 biological replicates. For 645, n = 3 biological replicates.

(F) Schematic for the OT-I T cell co-culture assay with 1014 cells expressing OVA pretreated with DMSO, IFNγ (10 ng/mL), LSN3321213 (125 nM), or LSN3321213 (125 nM) and IFNγ (10 ng/mL). E, effector (OT-I T cells); T, target (1014 OVA).

(G) Percentage tumor cell survival of 1014 OVA after 48-h co-culture with activated Cd8a+ T cells from OT-I mice at indicated effector/target (E/T) ratios. Each data point represents mean ± SEM. n = 2 independent biological replicates, each with three technical replicates. *p < 0.05, **p < 0.01, ***p < 0.001, ***p < 0.0001. Data are represented as mean ± SEM in (E) and (G). See also Figures S12–S20.

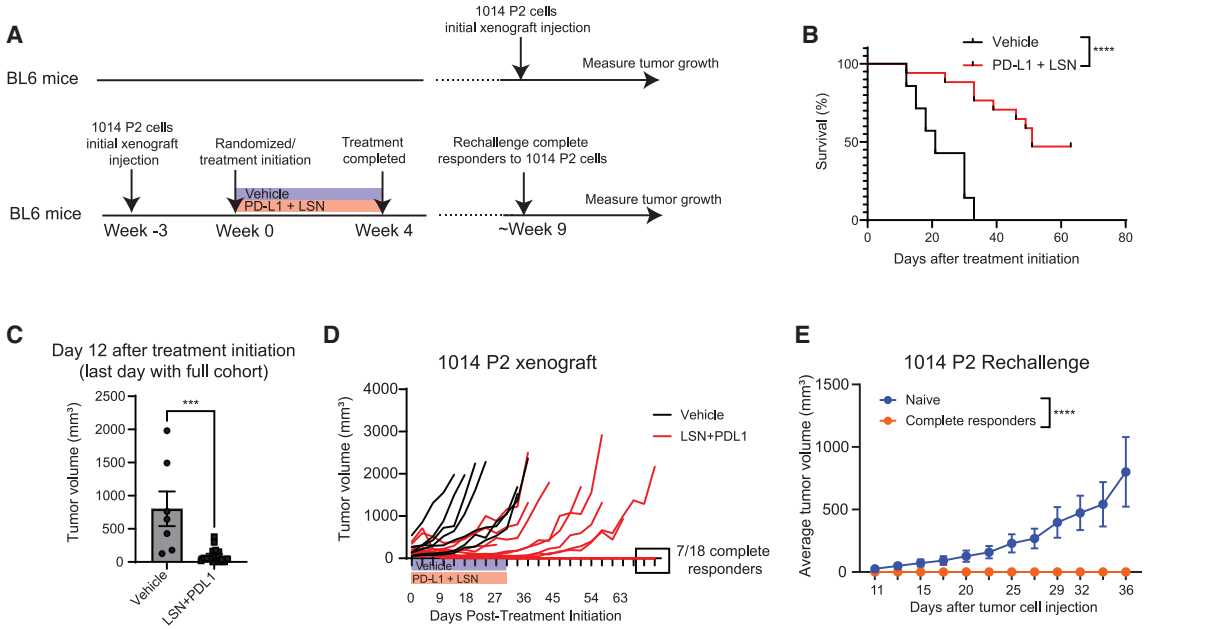

Figure 7. LSN3321213 and PD-L1 promotes protective immunity in mice

(A) Schematic for the *RPR2* 1014 P2 xenograft and subsequent re-challenge experiments. BL6 mice bearing *RPR2* 1014 P2 tumors were randomized (3:1) to vehicle (H_3PO_4) (n = 7) or combined LSN3321213 (57 mg/kg p.o. BID) and PD-L1 (200 μg/mouse 3×/week) (n = 18) for 28 days. Five weeks after completion of treatment, complete responders in the combined treatment group (n = 7) and age-matched tumor-naive BL6 mice (n = 10) were rechallenged with *RPR2* 1014 P2 cells.

(B) Kaplan-Meier survival of mice with *RPR2* 1014 P2 xenografts treated with vehicle or combined LSN3321213 and PD-L1. N = 7 mice (vehicle), n = 18 mice (LSN3321213 + PD-L1).

(C) Tumor volumes determined using calipers on day 12 (the last day that all mice were alive in both treatment groups) after treatment initiation.

(D) Spider plots of individual *RPR2* 1014 P2 xenograft tumors treated with vehicle (H_3PO_4) or combined LSN3321213 and PD-L1 for 28 days.

(E) Tumor volume measurements of complete responders or age-matched tumor-naive mice after subcutaneous *RPR2* 1014 P2 injection. n = 7 mice in complete responder group and n = 10 mice in age-matched naive BL6 controls. *p < 0.05, **p < 0.01, ***p < 0.001, ***p < 0.0001. Data are represented as mean ± SEM in (C) and (E). See also Figure S21.

DISCUSSION

Here, we find that the combination of a highly specific AURKAi LSN3321213, which is the erbumine salt of LY3295668 that has entered a clinical trial for SCLC[15] and PD-L1 ICB, together led to more durable anti-tumor efficacy in autochthonous and syngeneic xenograft immunocompetent SCLC mouse models of the ASCL1 subtype. Using scRNA-seq from tumors treated with LSN3321213, PD-L1, or both LSN3321213 and PD-L1, we found that LSN3321213 caused the accumulation of tumor cells in mitosis, which was expected given the known on-target mechanism of action of Aurora A kinase inhibition.[15,37] Surprisingly, we observed that expression patterns of tumor cells accumulated in mitosis is reminiscent of the recently described inflammatory SCLC subtype with low ASCL1 and high MHC-I and interferon target gene expression.[10,14] Together, our results suggest that a consequence of AURKAi blocking tumor cells in mitosis is to initiate conversion from an immune-cold tumor microenvironment to a tumor microenvironment with increased immune cell infiltration. This alone did not yield a durable anti-tumor immune response as the response is likely dampened by the PD-1/PD-L1 checkpoint. Addition of PD-L1 checkpoint inhibition to LSN3321213 induced more durable anti-tumor efficacy, leading to increased survival.

Consistent with our previous study showing tumor-cell-autonomous efficacy with selective AURKAi in immunocompromised patient-derived and cell line xenograft mouse models of SCLC,[15] here we observed efficacy after treatment with AURKAi alone at early time points in immunocompetent SCLC mouse models. The addition of PD-L1 added little to no additional benefit early on during treatment, suggesting that the initial responses were likely through tumor-cell-autonomous effects of AURKAi. However, the addition of PD-L1 to AURKAi increased the durability of response with several long-term responders leading to an improvement in overall survival. In line with our findings described above, a clinical trial of alisertib showed significant benefit of adding alisertib to paclitaxel in patients with *RB1* pathway mutations or MYC expression.[21] However, the PFS benefit was short lived, highlighting the need for new strategies to combine with AURKi to increase the durability of response and achieve more meaningful clinical activity for patients. The highly specific AURKAi LSN3321213[15] was dosed continuously in our study and was overall well tolerated alone or when combined with PD-L1, suggesting that combination approaches with LSN3321213 are feasible with other agents with non-overlapping toxicity. SCLC cell lines compared to many other cancer cell lines are more highly sensitive to AURKi because SCLC has near-universal LOF mutations in *RB1* and high expression of MYC,[15–19] which likely leads to a larger therapeutic index for SCLC *in vivo*. Consistent with this, lymphocytes within tumors did not accumulate in mitosis after LSN3321213 treatment, suggesting a therapeutic

window allowing for selective AURKAi in tumor cells while preserving the ability of lymphocytes to proliferate and promote an antitumor immune response. Future studies should continue to focus on optimal combination strategies with AURKi that promote antitumor efficacy through both tumor-cell-autonomous mechanisms and augmentation of immunotherapy efficacy. Our data suggest that AURKAi combined with PD-L1 is one strategy that could achieve this to improve the durability of response and should be explored further.

Aurora kinase inhibition has been shown to cooperate with ICB blockade in other mouse models of cancer, including breast cancer, lymphoma, and melanoma.[36,47,48] A recent study found that AURKAi cooperated with PD-1 by increasing PD-L1 expression on tumor cells primarily in cancer models with relatively high baseline PD-L1 expression.[49] Our study focused on ASCL1-positive SCLC, which is different from tumor types in the studies above in that SCLC tumor cells nearly completely silence PD-L1 and MHC-I expression at baseline.[50–52] Our results suggest a mechanism in SCLC linked to AURKAi blocking cells in mitosis and consequently upregulating expression of interferon signaling and antigen presentation, gene expression programs that more highly correlate with ICB-responsive human SCLCs.[10,13,14] Our results in cell lines suggest that other mitotic inhibitors can achieve this but this would need to be formally tested *in vivo*. Whether blocking cells in mitosis by AURKAi unmasks an inflammatory cell state in other tumor types is not known and an interesting area for future studies. A recent manuscript found that inhibition of WEE1, a G2/M checkpoint gatekeeper, caused accumulation of micronuclei leading to activation of the cGAS-STING pathway, induction of type I and type II interferons, and cooperated with PD-L1 using mostly non-ASCL1 subtype cell lines to uncover these mechanisms.[53] Hence, the mechanisms by which WEE1 inhibition and AURKAi cooperate with PD-L1 are likely distinct as we did not observe cGAS-STING pathway activation or tumor cell IFNγ production after AURKAi, although some of the differences between the studies could be related to the different SCLC subtype models examined.

Our study interrogates the native immune microenvironment in autochthonous murine SCLC lung tumors and identifies interactions between cells of the tumor microenvironment and SCLC tumor cells in GEMMs that are consistent with findings in human tumors. These include lack of PD-L1 expression on SCLC tumor cells with expression primarily on antigen-presenting cells[50–52] and $CD3^+$ T cells and NK cells as the primary source of IFNγ expression in the tumor microenvironment.[54] Our findings are also consistent with recent reports showing relative resistance of human SCLCs of the ASCL1 subtype to PD-L1[10,14] as PD-L1 ICB alone showed little efficacy in our SCLC immunocompetent models.

SCLC is a relatively immune-cold tumor with low MHC-I expression[9,55] and low inherent tumor immunogenicity. Recent research has focused on understanding SCLC molecular subtypes and each of their therapeutic vulnerabilities.[14] Our studies were performed with SCLCs of the ASCL1 subtype, which comprises ~60% of SCLCs[25] and typically repress genes involved in antigen presentation.[10,12,14] The NEUROD1 (~20%–30%) and POU2F3 (~10%–15%) subtypes are also inherently relatively resistant to PD-1/PD-L1 ICB.[14] Our study did not interrogate whether LSN3321213 + PD-L1 would be effective in NEUROD1 or POU2F3 subtypes and this can be explored in a future study. The fourth SCLC subtype, the inflammatory subtype[14] characterized by high MHC-I expression on tumor cells,[10] is significantly more ICB responsive, nominating the tumor cell inflammatory state with high MHC-I as a predictive biomarker of response to ICB. Recent studies found that EZH2 inhibitors[10,11] or LSD1 inhibitors[56,57] induce MHC-I expression and other changes toward a non-neuroendocrine inflammatory tumor cell state, which enhances the benefit of ICB in preclinical SCLC models. We find that a neuroendocrine-low, MHC-I-high tumor cell state can also be achieved by AURKAi, which traps cells in mitosis where they have lower ASCL1 and higher inflammatory gene expression, suggesting that a shift from an ASCL1 to inflammatory SCLC molecular cell state can also be achieved through targeting M phase arrest.

Limitations of the study

We focused on differences in MHC-I and inflammatory signaling in the M phase enriched tumor cell population based on our unbiased scRNA-seq cell-cell interaction analysis, the mechanism of action of LSN3321213, and the known correlation of SCLC inherent immunogenicity with features of molecular subtypes.[10,14] We cannot exclude the possibility that other mechanisms induced by AURKAi + PD-L1 in tumor cells contribute to efficacy, or that AURKAi also cooperates with PD-L1 by acting directly on other cells of the tumor immune microenvironment, such as was observed previously with myeloid cells.[36]

Another limitations is that our studies were performed using autochthonous GEMMs and syngeneic xenograft SCLC mouse models, which are powerful models to study the effect of a therapy or perturbation in a host with an intact immune system, but have several differences compared to their human cancer counterparts,[58] including a much lower mutational burden and hence a lower neo-antigen load. Although we did find that mice with a complete response to LSN3321213 + PD-L1 were able to reject subsequent SCLC tumor cell xenograft transplants, suggesting protective immunity, we could not identify enriched T cell clonotypes or the tumor cell antigen/s that were recognized in these mice as no tumors formed in the rechallenged mice. Although GEMMs and syngeneic models do have a lower mutational burden, we previously identified an antigen-specific T cell clone in BL6 mice that recognized non-neuroendocrine *RPR2* 631 cells with restored MHC I expression,[10] suggesting SCLC GEMMs are capable of eliciting an antigen-specific T cell response when MHC-I is restored despite their low mutational burden. Given the differences in mutational burden and neo-antigen load between mouse models and human tumors, it is very likely that different antigens will be presented by tumor cell MHC-I and recognized by T cells in human SCLCs. Identifying antigen-specific T cells and their tumor antigens in both mouse and human SCLCs will require future studies.

STAR★METHODS

Detailed methods are provided in the online version of this paper and include the following:

- KEY RESOURCES TABLE
- RESOURCE AVAILABILITY
  - Lead contact

SUPPLEMENTAL INFORMATION

Supplemental information can be found online at https://doi.org/10.1016/j.xcrm.2023.101282.

ACKNOWLEDGMENTS

We thank the members of the Oser, Barbie, and Janne laboratories for insightful discussions; the Expect Miracles Foundation; and the Robert A. and Renee E. Belfer Family Foundation. Figures 1D, 2A, 3A, S7A were created with BioRender.com.

Funding: this work was supported by a WAVE 5 grant funded by Loxo/Lilly (M.G.O.). M.G.O. is a William Raveis Charitable Fund Damon Runyon Clinical Investigator supported by the Damon Runyon Cancer Research Foundation (CI-101-19), an NCI/NIH K08 grant (no. K08CA222657), and the Kaplan Family Fund. S.L. is supported by the NCI Research Specialist Award (R50CA251956).

AUTHOR CONTRIBUTIONS

Conceptualization, Y.L. and M.G.O.; methodology, Y.L., L.D., D.H., P.C.G., Q.D.N., and M.G.O.; investigation, Y.L., N.R.M., L.D., D.H., Y.T.D., K.L.J., H.C., M.M., A.P., M.J.P., B.F.S., R.T.B., X.G., Y.H.H., J.D., J.S., T.T., S.L., and P.H.L.; formal analysis, Y.L., L.D., S.L., P.L., P.C.G., Q.D.N., and M.G.O.; writing, Y.L. and M.G.O.; review and editing, all authors; funding acquisition, M.G.O.

DECLARATION OF INTERESTS

M.G.O. reports grants from Eli Lilly, Takeda, Novartis, BMS, and Circle Pharma and is a consultant for Ananke therapeutics and Daiichi Sankyo. This work was funded by an Eli Lilly Wave 5 grant. X.G., Y.H.H., and J.D. are scientists at Eli Lilly and Company and have ownership of interest including patents and stocks.

Received: December 7, 2022
Revised: August 17, 2023
Accepted: October 16, 2023
Published: November 21, 2023

REFERENCES

1. Rudin, C.M., Brambilla, E., Faivre-Finn, C., and Sage, J. (2021). Small-cell lung cancer. Nat. Rev. Dis. Primers *7*, 3. https://doi.org/10.1038/s41572-020-00235-0.
2. Kalemkerian, G.P., Akerley, W., Bogner, P., Borghaei, H., Chow, L.Q., Downey, R.J., Gandhi, L., Ganti, A.K.P., Govindan, R., Grecula, J.C., et al. (2013). Small cell lung cancer. J. Natl. Compr. Canc. Netw. *11*, 78–98.
3. Horn, L., Mansfield, A.S., Szczęsna, A., Havel, L., Krzakowski, M., Hochmair, M.J., Huemer, F., Losonczy, G., Johnson, M.L., Nishio, M., et al. (2018). First-Line Atezolizumab plus Chemotherapy in Extensive-Stage Small-Cell Lung Cancer. N. Engl. J. Med. *379*, 2220–2229. https://doi.org/10.1056/NEJMoa1809064.
4. Paz-Ares, L., Dvorkin, M., Chen, Y., Reinmuth, N., Hotta, K., Trukhin, D., Statsenko, G., Hochmair, M.J., Özgüroğlu, M., Ji, J.H., et al. (2019). Durvalumab plus platinum-etoposide versus platinum-etoposide in first-line treatment of extensive-stage small-cell lung cancer (CASPIAN): a randomised, controlled, open-label, phase 3 trial. Lancet *394*, 1929–1939. https://doi.org/10.1016/S0140-6736(19)32222-6.
5. Yarchoan, M., Hopkins, A., and Jaffee, E.M. (2017). Tumor Mutational Burden and Response Rate to PD-1 Inhibition. N. Engl. J. Med. *377*, 2500–2501. https://doi.org/10.1056/NEJMc1713444.
6. Leone, P., Shin, E.C., Perosa, F., Vacca, A., Dammacco, F., and Racanelli, V. (2013). MHC class I antigen processing and presenting machinery: organization, function, and defects in tumor cells. J. Natl. Cancer Inst. *105*, 1172–1187. https://doi.org/10.1093/jnci/djt184.
7. Garrido, F., Aptsiauri, N., Doorduijn, E.M., Garcia Lora, A.M., and van Hall, T. (2016). The urgent need to recover MHC class I in cancers for effective immunotherapy. Curr. Opin. Immunol. *39*, 44–51. https://doi.org/10.1016/j.coi.2015.12.007.
8. Zaretsky, J.M., Garcia-Diaz, A., Shin, D.S., Escuin-Ordinas, H., Hugo, W., Hu-Lieskovan, S., Torrejon, D.Y., Abril-Rodriguez, G., Sandoval, S., Barthly, L., et al. (2016). Mutations Associated with Acquired Resistance

to PD-1 Blockade in Melanoma. N. Engl. J. Med. *375*, 819–829. https://doi.org/10.1056/NEJMoa1604958.

9. Chen, H.L., Gabrilovich, D., Tampé, R., Girgis, K.R., Nadaf, S., and Carbone, D.P. (1996). A functionally defective allele of TAP1 results in loss of MHC class I antigen presentation in a human lung cancer. Nat. Genet. *13*, 210–213. https://doi.org/10.1038/ng0696-210.
10. Mahadevan, N.R., Knelson, E.H., Wolff, J.O., Vajdi, A., Saigí, M., Campisi, M., Hong, D., Thai, T.C., Piel, B., Han, S., et al. (2021). Intrinsic immunogenicity of small cell lung carcinoma revealed by its cellular plasticity. Cancer Discov. *11*, 1952–1969. https://doi.org/10.1158/2159-8290.CD-20-0913.
11. Burr, M.L., Sparbier, C.E., Chan, K.L., Chan, Y.C., Kersbergen, A., Lam, E.Y.N., Azidis-Yates, E., Vassiliadis, D., Bell, C.C., Gilan, O., et al. (2019). An Evolutionarily Conserved Function of Polycomb Silences the MHC Class I Antigen Presentation Pathway and Enables Immune Evasion in Cancer. Cancer Cell *36*, 385–401.e8. https://doi.org/10.1016/j.ccell.2019.08.008.
12. Cai, L., Liu, H., Huang, F., Fujimoto, J., Girard, L., Chen, J., Li, Y., Zhang, Y.A., Deb, D., Stastny, V., et al. (2021). Cell-autonomous immune gene expression is repressed in pulmonary neuroendocrine cells and small cell lung cancer. Commun. Biol. *4*, 314. https://doi.org/10.1038/s42003-021-01842-7.
13. Rudin, C.M., Balli, D., Lai, W.V., Richards, A.L., Nguyen, E., Egger, J.V., Choudhury, N.J., Sen, T., Chow, A., Poirier, J.T., et al. (2023). Clinical benefit from immunotherapy in patients with small cell lung cancer is associated with tumor capacity for antigen presentation. J. Thorac. Oncol. *18*, 1222–1232. https://doi.org/10.1016/j.jtho.2023.05.008.
14. Gay, C.M., Stewart, C.A., Park, E.M., Diao, L., Groves, S.M., Heeke, S., Nabet, B.Y., Fujimoto, J., Solis, L.M., Lu, W., et al. (2021). Patterns of transcription factor programs and immune pathway activation define four major subtypes of SCLC with distinct therapeutic vulnerabilities. Cancer Cell *39*, 346–360.e7. https://doi.org/10.1016/j.ccell.2020.12.014.
15. Gong, X., Du, J., Parsons, S.H., Merzoug, F.F., Webster, Y., Iversen, P.W., Chio, L.C., Van Horn, R.D., Lin, X., Blosser, W., et al. (2019). Aurora A Kinase Inhibition Is Synthetic Lethal with Loss of the RB1 Tumor Suppressor Gene. Cancer Discov. *9*, 248–263. https://doi.org/10.1158/2159-8290.CD-18-0469.
16. Oser, M.G., Fonseca, R., Chakraborty, A.A., Brough, R., Spektor, A., Jennings, R.B., Flaifel, A., Novak, J.S., Gulati, A., Buss, E., et al. (2019). Cells Lacking the RB1 Tumor Suppressor Gene Are Hyperdependent on Aurora B Kinase for Survival. Cancer Discov. *9*, 230–247. https://doi.org/10.1158/2159-8290.CD-18-0389.
17. Sos, M.L., Dietlein, F., Peifer, M., Schöttle, J., Balke-Want, H., Müller, C., Koker, M., Richters, A., Heynck, S., Malchers, F., et al. (2012). A framework for identification of actionable cancer genome dependencies in small cell lung cancer. Proc. Natl. Acad. Sci. USA *109*, 17034–17039. https://doi.org/10.1073/pnas.1207310109.
18. Mollaoglu, G., Guthrie, M.R., Böhm, S., Brägelmann, J., Can, I., Ballieu, P.M., Marx, A., George, J., Heinen, C., Chalishazar, M.D., et al. (2017). MYC Drives Progression of Small Cell Lung Cancer to a Variant Neuroendocrine Subtype with Vulnerability to Aurora Kinase Inhibition. Cancer Cell *31*, 270–285. https://doi.org/10.1016/j.ccell.2016.12.005.
19. Helfrich, B.A., Kim, J., Gao, D., Chan, D.C., Zhang, Z., Tan, A.C., and Bunn, P.A., Jr. (2016). Barasertib (AZD1152), a Small Molecule Aurora B Inhibitor, Inhibits the Growth of SCLC Cell Lines In Vitro and In Vivo. Mol. Cancer Ther. *15*, 2314–2322. https://doi.org/10.1158/1535-7163.MCT-16-0298.
20. Dammert, M.A., Brägelmann, J., Olsen, R.R., Böhm, S., Monhasery, N., Whitney, C.P., Chalishazar, M.D., Tumbrink, H.L., Guthrie, M.R., Klein, S., et al. (2019). MYC paralog-dependent apoptotic priming orchestrates a spectrum of vulnerabilities in small cell lung cancer. Nat. Commun. *10*, 3485. https://doi.org/10.1038/s41467-019-11371-x.
21. Owonikoko, T.K., Niu, H., Nackaerts, K., Csoszi, T., Ostoros, G., Mark, Z., Baik, C., Joy, A.A., Chouaid, C., Jaime, J.C., et al. (2020). Randomized Phase II Study of Paclitaxel plus Alisertib versus Paclitaxel plus Placebo as Second-Line Therapy for SCLC: Primary and Correlative Biomarker Analyses. J. Thorac. Oncol. *15*, 274–287. https://doi.org/10.1016/j.jtho.2019.10.013.
22. Oser, M.G., Sabet, A.H., Gao, W., Chakraborty, A.A., Schinzel, A.C., Jennings, R.B., Fonseca, R., Bonal, D.M., Booker, M.A., Flaifel, A., et al. (2019). The KDM5A/RBP2 histone demethylase represses NOTCH signaling to sustain neuroendocrine differentiation and promote small cell lung cancer tumorigenesis. Genes Dev. *33*, 1718–1738. https://doi.org/10.1101/gad.328336.119.
23. Hong, D., Knelson, E.H., Li, Y., Durmaz, Y.T., Gao, W., Walton, E., Vajdi, A., Thai, T., Sticco-Ivins, M., Sabet, A.H., et al. (2022). Plasticity in the Absence of NOTCH Uncovers a RUNX2-Dependent Pathway in Small Cell Lung Cancer. Cancer Res. *82*, 248–263. https://doi.org/10.1158/0008-5472.CAN-21-1991.
24. Zhang, H., Christensen, C.L., Dries, R., Oser, M.G., Deng, J., Diskin, B., Li, F., Pan, Y., Zhang, X., Yin, Y., et al. (2020). CDK7 Inhibition Potentiates Genome Instability Triggering Anti-tumor Immunity in Small Cell Lung Cancer. Cancer Cell *37*, 37–54.e9. https://doi.org/10.1016/j.ccell.2019.11.003.
25. Rudin, C.M., Poirier, J.T., Byers, L.A., Dive, C., Dowlati, A., George, J., Heymach, J.V., Johnson, J.E., Lehman, J.M., MacPherson, D., et al. (2019). Molecular subtypes of small cell lung cancer: a synthesis of human and mouse model data. Nat. Rev. Cancer *19*, 289–297. https://doi.org/10.1038/s41568-019-0133-9.
26. Pardoll, D.M., and Topalian, S.L. (1998). The role of CD4+ T cell responses in antitumor immunity. Curr. Opin. Immunol. *10*, 588–594. https://doi.org/10.1016/s0952-7915(98)80228-8.
27. Corthay, A., Skovseth, D.K., Lundin, K.U., Røsjø, E., Omholt, H., Hofgaard, P.O., Haraldsen, G., and Bogen, B. (2005). Primary antitumor immune response mediated by CD4+ T cells. Immunity *22*, 371–383. https://doi.org/10.1016/j.immuni.2005.02.003.
28. Farhood, B., Najafi, M., and Mortezaee, K. (2019). CD8(+) cytotoxic T lymphocytes in cancer immunotherapy: A review. J. Cell. Physiol. *234*, 8509–8521. https://doi.org/10.1002/jcp.27782.
29. Raskov, H., Orhan, A., Christensen, J.P., and Gögenur, I. (2021). Cytotoxic CD8(+) T cells in cancer and cancer immunotherapy. Br. J. Cancer *124*, 359–367. https://doi.org/10.1038/s41416-020-01048-4.
30. Hervas-Stubbs, S., Mancheño, U., Riezu-Boj, J.I., Larraga, A., Ochoa, M.C., Alignani, D., Alfaro, C., Morales-Kastresana, A., Gonzalez, I., Larrea, E., et al. (2012). CD8 T cell priming in the presence of IFN-alpha renders CTLs with improved responsiveness to homeostatic cytokines and recall antigens: important traits for adoptive T cell therapy. J. Immunol. *189*, 3299–3310. https://doi.org/10.4049/jimmunol.1102495.
31. Ontiveros, F., Wilson, E.B., and Livingstone, A.M. (2011). Type I interferon supports primary CD8+ T-cell responses to peptide-pulsed dendritic cells in the absence of CD4+ T-cell help. Immunology *132*, 549–558. https://doi.org/10.1111/j.1365-2567.2010.03400.x.
32. Devaud, C., Westwood, J.A., John, L.B., Flynn, J.K., Paquet-Fifield, S., Duong, C.P.M., Yong, C.S.M., Pegram, H.J., Stacker, S.A., Achen, M.G., et al. (2014). Tissues in different anatomical sites can sculpt and vary the tumor microenvironment to affect responses to therapy. Mol. Ther. *22*, 18–27. https://doi.org/10.1038/mt.2013.219.
33. Fung, A.S., Lee, C., Yu, M., and Tannock, I.F. (2015). The effect of chemotherapeutic agents on tumor vasculature in subcutaneous and orthotopic human tumor xenografts. BMC Cancer *15*, 112. https://doi.org/10.1186/s12885-015-1091-6.
34. Guerin, M.V., Finisguerra, V., Van den Eynde, B.J., Bercovici, N., and Trautmann, A. (2020). Preclinical murine tumor models: a structural and functional perspective. Elife *9*, e50740. https://doi.org/10.7554/eLife.50740.
35. Altorki, N.K., Markowitz, G.J., Gao, D., Port, J.L., Saxena, A., Stiles, B., McGraw, T., and Mittal, V. (2019). The lung microenvironment: an important regulator of tumour growth and metastasis. Nat. Rev. Cancer *19*, 9–31. https://doi.org/10.1038/s41568-018-0081-9.
36. Yin, T., Zhao, Z.B., Guo, J., Wang, T., Yang, J.B., Wang, C., Long, J., Ma, S., Huang, Q., Zhang, K., et al. (2019). Aurora A Inhibition Eliminates Myeloid Cell-Mediated Immunosuppression and Enhances the Efficacy of Anti-PD-L1 Therapy in Breast Cancer. Cancer Res. *79*, 3431–3444. https://doi.org/10.1158/0008-5472.CAN-18-3397.

37. Du, J., Yan, L., Torres, R., Gong, X., Bian, H., Marugán, C., Boehnke, K., Baquero, C., Hui, Y.H., Chapman, S.C., et al. (2019). Aurora A-Selective Inhibitor LY3295668 Leads to Dominant Mitotic Arrest, Apoptosis in Cancer Cells, and Shows Potent Preclinical Antitumor Efficacy. Mol. Cancer Ther. *18*, 2207–2219. https://doi.org/10.1158/1535-7163.MCT-18-0529.

38. Bavetsias, V., and Linardopoulos, S. (2015). Aurora Kinase Inhibitors: Current Status and Outlook. Front. Oncol. *5*, 278. https://doi.org/10.3389/fonc.2015.00278.

39. Browaeys, R., Saelens, W., and Saeys, Y. (2020). NicheNet: modeling intercellular communication by linking ligands to target genes. Nat. Methods *17*, 159–162. https://doi.org/10.1038/s41592-019-0667-5.

40. Cullen, S.P., Brunet, M., and Martin, S.J. (2010). Granzymes in cancer and immunity. Cell Death Differ. *17*, 616–623. https://doi.org/10.1038/cdd.2009.206.

41. House, I.G., Savas, P., Lai, J., Chen, A.X.Y., Oliver, A.J., Teo, Z.L., Todd, K.L., Henderson, M.A., Giuffrida, L., Petley, E.V., et al. (2020). Macrophage-Derived CXCL9 and CXCL10 Are Required for Antitumor Immune Responses Following Immune Checkpoint Blockade. Clin. Cancer Res. *26*, 487–504. https://doi.org/10.1158/1078-0432.CCR-19-1868.

42. Tokunaga, R., Zhang, W., Naseem, M., Puccini, A., Berger, M.D., Soni, S., McSkane, M., Baba, H., and Lenz, H.J. (2018). CXCL9, CXCL10, CXCL11/CXCR3 axis for immune activation - A target for novel cancer therapy. Cancer Treat Rev. *63*, 40–47. https://doi.org/10.1016/j.ctrv.2017.11.007.

43. Zitvogel, L., Galluzzi, L., Kepp, O., Smyth, M.J., and Kroemer, G. (2015). Type I interferons in anticancer immunity. Nat. Rev. Immunol. *15*, 405–414. https://doi.org/10.1038/nri3845.

44. Shen, J., Ju, Z., Zhao, W., Wang, L., Peng, Y., Ge, Z., Nagel, Z.D., Zou, J., Wang, C., Kapoor, P., et al. (2018). ARID1A deficiency promotes mutability and potentiates therapeutic antitumor immunity unleashed by immune checkpoint blockade. Nat. Med. *24*, 556–562. https://doi.org/10.1038/s41591-018-0012-z.

45. Sade-Feldman, M., Jiao, Y.J., Chen, J.H., Rooney, M.S., Barzily-Rokni, M., Eliane, J.P., Bjorgaard, S.L., Hammond, M.R., Vitzthum, H., Blackmon, S.M., et al. (2017). Resistance to checkpoint blockade therapy through inactivation of antigen presentation. Nat. Commun. *8*, 1136. https://doi.org/10.1038/s41467-017-01062-w.

46. Torrejon, D.Y., Abril-Rodriguez, G., Champhekar, A.S., Tsoi, J., Campbell, K.M., Kalbasi, A., Parisi, G., Zaretsky, J.M., Garcia-Diaz, A., Puig-Saus, C., et al. (2020). Overcoming Genetically Based Resistance Mechanisms to PD-1 Blockade. Cancer Discov. *10*, 1140–1157. https://doi.org/10.1158/2159-8290.CD-19-1409.

47. Punt, S., Malu, S., McKenzie, J.A., Manrique, S.Z., Doorduijn, E.M., Mbofung, R.M., Williams, L., Silverman, D.A., Ashkin, E.L., Dominguez, A.L., et al. (2021). Aurora kinase inhibition sensitizes melanoma cells to T-cell-mediated cytotoxicity. Cancer Immunol. Immunother. *70*, 1101–1113. https://doi.org/10.1007/s00262-020-02748-9.

48. Islam, S., Vick, E., Huber, B., Morales, C., Spier, C., Cooke, L., Weterings, E., and Mahadevan, D. (2017). Co-targeting aurora kinase with PD-L1 and PI3K abrogates immune checkpoint mediated proliferation in peripheral T-cell lymphoma: a novel therapeutic strategy. Oncotarget *8*, 100326–100338. https://doi.org/10.18632/oncotarget.22222.

49. Wang, X., Huang, J., Liu, F., Yu, Q., Wang, R., Wang, J., Zhu, Z., Yu, J., Hou, J., Shim, J.S., et al. (2023). Aurora A kinase inhibition compromises its antitumor efficacy by elevating PD-L1 expression. J. Clin. Invest. *133*, e161929. https://doi.org/10.1172/JCI161929.

50. Guleria, P., Kumar, S., Malik, P.S., and Jain, D. (2020). PD-L1 Expression in Small Cell and Large Cell Neuroendocrine Carcinomas of Lung: an Immunohistochemical Study with Review of Literature. Pathol. Oncol. Res. *26*, 2363–2370. https://doi.org/10.1007/s12253-020-00832-0.

51. Schultheis, A.M., Scheel, A.H., Ozretić, L., George, J., Thomas, R.K., Hagemann, T., Zander, T., Wolf, J., and Buettner, R. (2015). PD-L1 expression in small cell neuroendocrine carcinomas. Eur. J. Cancer *51*, 421–426. https://doi.org/10.1016/j.ejca.2014.12.006.

52. Yasuda, Y., Ozasa, H., and Kim, Y.H. (2018). PD-L1 Expression in Small Cell Lung Cancer. J. Thorac. Oncol. *13*, e40–e41. https://doi.org/10.1016/j.jtho.2017.10.013.

53. Taniguchi, H., Caeser, R., Chavan, S.S., Zhan, Y.A., Chow, A., Manoj, P., Uddin, F., Kitai, H., Qu, R., Hayatt, O., et al. (2022). WEE1 inhibition enhances the antitumor immune response to PD-L1 blockade by the concomitant activation of STING and STAT1 pathways in SCLC. Cell Rep. *39*, 110814. https://doi.org/10.1016/j.celrep.2022.110814.

54. Alspach, E., Lussier, D.M., and Schreiber, R.D. (2019). Interferon gamma and Its Important Roles in Promoting and Inhibiting Spontaneous and Therapeutic Cancer Immunity. Cold Spring Harb. Perspect. Biol. *11*, a028480. https://doi.org/10.1101/cshperspect.a028480.

55. Doyle, A., Martin, W.J., Funa, K., Gazdar, A., Carney, D., Martin, S.E., Linnoila, I., Cuttitta, F., Mulshine, J., Bunn, P., et al. (1985). Markedly decreased expression of class I histocompatibility antigens, protein, and mRNA in human small-cell lung cancer. J. Exp. Med. *161*, 1135–1151. https://doi.org/10.1084/jem.161.5.1135.

56. Hiatt, J.B., Sandborg, H., Garrison, S.M., Arnold, H.U., Liao, S.Y., Norton, J.P., Friesen, T.J., Wu, F., Sutherland, K.D., Rienhoff, H.Y., et al. (2022). Inhibition of LSD1 with Bomedemstat Sensitizes Small Cell Lung Cancer to Immune Checkpoint Blockade and T-Cell Killing. Clin. Cancer Res. *28*, 4551–4564. https://doi.org/10.1158/1078-0432.CCR-22-1128.

57. Nguyen, E.M., Taniguchi, H., Chan, J.M., Zhan, Y.A., Chen, X., Qiu, J., de Stanchina, E., Allaj, V., Shah, N.S., Uddin, F., et al. (2022). Targeting Lysine-Specific Demethylase 1 Rescues Major Histocompatibility Complex Class I Antigen Presentation and Overcomes Programmed Death-Ligand 1 Blockade Resistance in SCLC. J. Thorac. Oncol. *17*, 1014–1031. https://doi.org/10.1016/j.jtho.2022.05.014.

58. McFadden, D.G., Politi, K., Bhutkar, A., Chen, F.K., Song, X., Pirun, M., Santiago, P.M., Kim-Kiselak, C., Platt, J.T., Lee, E., et al. (2016). Mutational landscape of EGFR-MYC-and Kras-driven genetically engineered mouse models of lung adenocarcinoma. Proc. Natl. Acad. Sci. USA *113*, E6409–E6417. https://doi.org/10.1073/pnas.1613601113.

59. Tirosh, I., Izar, B., Prakadan, S.M., Wadsworth, M.H., 2nd, Treacy, D., Trombetta, J.J., Rotem, A., Rodman, C., Lian, C., Murphy, G., et al. (2016). Dissecting the multicellular ecosystem of metastatic melanoma by single-cell RNA-seq. Science *352*, 189–196. https://doi.org/10.1126/science.aad0501.

60. Tanenbaum, M.E., Stern-Ginossar, N., Weissman, J.S., and Vale, R.D. (2015). Regulation of mRNA translation during mitosis. Elife *4*, e07957. https://doi.org/10.7554/eLife.07957.

61. Hao, Y., Hao, S., Andersen-Nissen, E., Mauck, W.M., 3rd, Zheng, S., Butler, A., Lee, M.J., Wilk, A.J., Darby, C., Zager, M., et al. (2021). Integrated analysis of multimodal single-cell data. Cell *184*, 3573–3587.e29. https://doi.org/10.1016/j.cell.2021.04.048.

62. Subramanian, A., Tamayo, P., Mootha, V.K., Mukherjee, S., Ebert, B.L., Gillette, M.A., Paulovich, A., Pomeroy, S.L., Golub, T.R., Lander, E.S., and Mesirov, J.P. (2005). Gene set enrichment analysis: a knowledge-based approach for interpreting genome-wide expression profiles. Proc. Natl. Acad. Sci. USA *102*, 15545–15550. https://doi.org/10.1073/pnas.0506580102.

63. DuPage, M., Dooley, A.L., and Jacks, T. (2009). Conditional mouse lung cancer models using adenoviral or lentiviral delivery of Cre recombinase. Nat. Protoc. *4*, 1064–1072. https://doi.org/10.1038/nprot.2009.95.

64. Wu, J., and Houghton, P.J. (2010). Interval approach to assessing antitumor activity for tumor xenograft studies. Pharm. Stat. *9*, 46–54. https://doi.org/10.1002/pst.369.

65. Duplaquet, L., Li, Y., Booker, M.A., Xie, Y., Olsen, S.N., Patel, R.A., Hong, D., Hatton, C., Denize, T., Walton, E., et al. (2023). KDM6A epigenetically regulates subtype plasticity in small cell lung cancer. Nat. Cell Biol. *25*, 1346–1358. https://doi.org/10.1038/s41556-023-01210-z.

66. Platt, R.J., Chen, S., Zhou, Y., Yim, M.J., Swiech, L., Kempton, H.R., Dahlman, J.E., Parnas, O., Eisenhaure, T.M., Jovanovic, M., et al. (2014).

CRISPR-Cas9 knockin mice for genome editing and cancer modeling. Cell *159*, 440–455. https://doi.org/10.1016/j.cell.2014.09.014.

67. Aran, D., Looney, A.P., Liu, L., Wu, E., Fong, V., Hsu, A., Chak, S., Naikawadi, R.P., Wolters, P.J., Abate, A.R., et al. (2019). Reference-based analysis of lung single-cell sequencing reveals a transitional profibrotic macrophage. Nat. Immunol. *20*, 163–172. https://doi.org/10.1038/s41590-018-0276-y.
68. Heng, T.S.P., and Painter, M.W.; Immunological Genome Project Consortium (2008). The Immunological Genome Project: networks of gene expression in immune cells. Nat. Immunol. *9*, 1091–1094. https://doi.org/10.1038/ni1008-1091.
69. Benayoun, B.A., Pollina, E.A., Singh, P.P., Mahmoudi, S., Harel, I., Casey, K.M., Dulken, B.W., Kundaje, A., and Brunet, A. (2019). Remodeling of epigenome and transcriptome landscapes with aging in mice reveals widespread induction of inflammatory responses. Genome Res. *29*, 697–709. https://doi.org/10.1101/gr.240093.118.
70. O'Connor, S.A., Feldman, H.M., Arora, S., Hoellerbauer, P., Toledo, C.M., Corrin, P., Carter, L., Kufeld, M., Bolouri, H., Basom, R., et al. (2021). Neural G0: a quiescent-like state found in neuroepithelial-derived cells and glioma. Mol. Syst. Biol. *17*, e9522. https://doi.org/10.15252/msb.20209522.
71. Yu, G., Wang, L.G., Han, Y., and He, Q.Y. (2012). clusterProfiler: an R package for comparing biological themes among gene clusters. OMICS *16*, 284–287. https://doi.org/10.1089/omi.2011.0118.
72. Lizotte, P.H., Hong, R.L., Luster, T.A., Cavanaugh, M.E., Taus, L.J., Wang, S., Dhaneshwar, A., Mayman, N., Yang, A., Kulkarni, M., et al. (2018). A High-Throughput Immune-Oncology Screen Identifies EGFR Inhibitors as Potent Enhancers of Antigen-Specific Cytotoxic T-lymphocyte Tumor Cell Killing. Cancer Immunol. Res. *6*, 1511–1523. https://doi.org/10.1158/2326-6066.CIR-18-0193.
73. Borromeo, M.D., Savage, T.K., Kollipara, R.K., He, M., Augustyn, A., Osborne, J.K., Girard, L., Minna, J.D., Gazdar, A.F., Cobb, M.H., and Johnson, J.E. (2016). ASCL1 and NEUROD1 Reveal Heterogeneity in Pulmonary Neuroendocrine Tumors and Regulate Distinct Genetic Programs. Cell Rep. *16*, 1259–1272. https://doi.org/10.1016/j.celrep.2016.06.081.

STAR★METHODS

KEY RESOURCES TABLE

REAGENT or RESOURCE	SOURCE	IDENTIFIER
Antibodies		
PE anti-mouse H-2L^{d}/H-2D^{b} Antibody	Biolegend	Cat#114507 (clone: 28-14-8); RRID:AB_313588
Pacific Blue anti-mouse H-2K^{b}	Biolegend	Cat#116514 (clone: AF6-88.5); RRID:AB_1967129
APC anti-mouse H-2K^{b} bound to SIINFEKL	Biolegend	Cat#141606 (clone: 25-D1.16); RRID:AB_11219595
PE Mouse IgG2a, κ Isotype Ctrl Antibody	Biolegend	Cat#400211 (clone: MOPC-173); RRID:AB_326460
Pacific Blue™ Mouse IgG2a, κ Isotype Ctrl Antibody	Biolegend	Cat#400235 (clone: MOPC-173)
APC Mouse IgG1, κ Isotype Ctrl Antibody	Biolegend	Cat#400119 (clone: MOPC-21); RRID:AB_2888687
PE anti-human HLA-A,B,C Antibody	Biolegend	Cat#311406 (clone: W6/32); RRID:AB_314875
PE Mouse IgG2a, κ Isotype Ctrl (FC) Antibody	Biolegend	Cat#400214 (clone: MOPC-173); RRID:AB_493447
Alexa Fluor® 488 anti-mouse/ human CD44 Antibody	Biolegend	Cat#103015 (clone: IM7); RRID:AB_493678
PerCP/Cyanine5.5 anti-mouse CD49b (pan-NK cells) Antibody	Biolegend	Cat#108916 (clone: DX5); RRID:AB_2129358
PE/Dazzle™ 594 anti-mouse CD8a Antibody	Biolegend	Cat#100762 (clone: 53-6.7); RRID:AB_2564027
Alexa Fluor® 700 anti-mouse CD3 Antibody	Biolegend	Cat#100216 (clone: 17A2); RRID:AB_493697
Brilliant Violet 421™ anti-mouse CD279 (PD-1) Antibody	Biolegend	Cat#109121 (clone: RMP1-30); RRID:AB_2687080
Brilliant Violet 510™ anti-mouse CD45 Antibody	Biolegend	Cat#103138 (clone: 30-F11); RRID:AB_2563061
Brilliant Violet 570™ anti-mouse CD62L	Biolegend	Cat#104433 (clone: MEL-14); RRID:AB_10900262
Brilliant Violet 605™ anti-mouse CD19 Antibody	Biolegend	Cat#115539 (clone: 6D5); RRID:AB_11203538
Brilliant Violet 711™ anti-mouse CD4 Antibody	Biolegend	Cat#100447 (clone: GK1.5); RRID:AB_2564586
FITC anti-mouse Ly-6C Antibody	Biolegend	Cat#128006 (clone: HK1.4); RRID:AB_1186135
PerCP/Cyanine5.5 anti-mouse Ly-6G Antibody	Biolegend	Cat#127615 (clone: 1A8); RRID:AB_1877272
PE/Cyanine7 anti-mouse CD68 Antibody	Biolegend	Cat#137015 (clone: FA-11); RRID:AB_2562947
Brilliant Violet 421™ anti-mouse CD274 (B7-H1, PD-L1) Antibody	Biolegend	Cat#124315 (clone: 10F.9G2); RRID:AB_10897097
Brilliant Violet 570™ anti-mouse CD11c Antibody	Biolegend	Cat#117331 (clone: N418); RRID:AB_10900261
Brilliant Violet 711™ anti-mouse/human CD11b Antibody	Biolegend	Cat#101241 (clone: M1/70); RRID:AB_11218791
Brilliant Violet 785™ anti-mouse F4/80 Antibody	Biolegend	Cat#123141 (clone: BM8); RRID:AB_2563667

(*Continued on next page*)

Continued

REAGENT or RESOURCE	SOURCE	IDENTIFIER
Phospho-Aurora A (Thr288)/Aurora B (Thr232)/Aurora C (Thr198)	Cell Signaling Technology	Cat#2914; RRID:AB_2061631
Recombinant Anti-MASH1/Achaete-scute homolog 1 antibody	Abcam	Cat#ab211327; RRID:AB_2924270
TAP1	Cell Signaling Technology	Cat#12341; RRID:AB_2797889
Monoclonal Anti-Vinculin antibody produced in mouse	Sigma Aldrich	Cat#V9131; RRID:AB_477629
Bacterial and virus strains		
HB-101	Promega	Cat#L2011
Chemicals, peptides, and recombinant proteins		
MK-5108	Selleckchem	Cat#S1166
AZD2811	Selleckchem	Cat#S1147
Paclitaxel	Selleckchem	Cat#S1150
PD-L1 antibody	Bio X Cell	Cat#BP0101 (clone: 10F.9G2)
LSN3321213	Eli Lilly and Company (obtained under an MTA)	N/A
Recombinant Mouse IFN-gamma Protein	R&D Systems	Cat#485-MI
Critical commercial assays		
Virabind Adenovirus Purification Kit	Cell Biolabs	Cat#VPK-5112
QuickTiter Adenovirus Quantitation Kit	Cell Biolabs	Cat#VPK-106
Mouse Tumor Dissociation Kit	Miltenyi Biotec	Cat#130-096-730
Chromium Next GEM Single Cell 5′ Kit v2 kit	10× Genomics	Cat#PN-1000263
RNeasy mini kit	Qiagen	Cat#74104
Dynabeads Mouse T-Activator CD3/CD28 beads	Thermo Fisher Scientific	Cat#11456D
CD8a (Ly-2) MicroBeads	Miltenyi Biotec	Cat#130-049-401
Deposited data		
Raw and processed single-cell RNA-sequencing and bulk RNA-sequencing data	This manuscript	GEO: GSE214614
Differentially expressed genes in tumor cells treated with LSN3321213 and PD-L1 or LSN3321213 alone compared to vehicle from single-cell RNA-seq	This manuscript	Table S4
FPKM values from bulk RNA-seq of tumors treated with LSN3321213 compared to vehicle	This manuscript	Table S5
Cell-cycle specific gene lists	Tirosh et al.[59]	Table S6
Top 50 upregulated genes in G2 phase vs. M phase	Tanenbaum et al.[60]	Table S7
Human MHC I high and low SCLC tumor samples transcriptomic profile	Mahadevan et al.[10]	GEO: GSE168295
Experimental models: Cell lines		
DMS 79	Dr. Kwok-kin Wong's laboratory	RRID:CVCL_1178
NCI-H69	American Type Culture Collection	RRID:CVCL_1579
1014 cells	Mouse SCLC tumor #1014	1014
1015 cells	Mouse SCLC tumor #1015	1015
645 cells	Mouse SCLC tumor #645	645
631 cells	Mouse SCLC tumor #631	631
159-1 cells	Mouse SCLC tumor #159-1	159–1

(*Continued on next page*)

Continued

REAGENT or RESOURCE	SOURCE	IDENTIFIER
Experimental models: Organisms/strains		
Rosa26-LSL-Cas9 knockin on B6J	Jackson Labs	Strain#026175; RRID:IMSR_JAX:026175
C57BL/6J-Tyrc-2J	Jackson Labs	Strain#000058; RRID:IMSR_JAX:000058
C57BL/6-Tg (TcraTcrb)1100Mjb/J OT-I mice	Jackson Labs	Strain#003831; RRID:IMSR_JAX:003831
Oligonucleotides		
sgRNA oligos	ADT	Table S8
B2m mouse RT-qPCR primer-Forward	5′ GTGACCCTGGTCTTTCTGGT 3′	N/A
B2m mouse RT-qPCR primer-Reverse	5′ GTATGTTCGGCTTCCCATTC 3′	N/A
36b4 mouse RT-qPCR primer-Forward	5′ CTGTTGGCCAATAAGGTGCC 3′	N/A
36b4 mouse RT-qPCR primer-Reverse	5′ GTTCTGAGCTGGCACAGTGA 3′	N/A
Recombinant DNA		
Adenovirus vector pAd/PL	Invitrogen	Cat#V494-20
psPAX2	Addgene	#12260
pMD2.G	Addgene	#12259
Software and algorithms		
Cell ranger pipeline Version 6.0.2	10× Genomics	https://support.10xgenomics.com/single-cell-gene-expression/software/pipelines/latest/installation
Seurat R package Version 4.1.0	Hao et al. Integrated analysis of multimodal single-cell data. Cell (2021) [Seurat V4][61]	https://satijalab.org/seurat/
Nichenetr R package Version 1.1.0	Browaeys et al., NicheNet: modeling intercellular communication by linking ligands to target genes. Nat Methods (2019)[39]	https://github.com/saeyslab/nichenetr
Gene Set Enrichment Analysis (GSEA)	Subramanian et al., 2005[62]	http://www.broad.mit.edu/gsea/downloads.jsp
FlowJo v10.5.3	FlowJo, LLC	https://www.flowjo.com/
Graphpad Prism 10	Graphpad	https://www.graphpad.com/

RESOURCE AVAILABILITY

Lead contact

Further information and requests for resources and reagents should be directed to and will be fulfilled by the lead contact, Matthew G. Oser (matthew_oser@dfci.harvard.edu).

Materials availability

This study did not generate new unique reagents.

Data and code availability

- Raw and processed single cell RNA-seq and bulk RNA-seq data have been deposited at NCBI GEO database and are publicly available (GSE214614). This paper also analyzes existing, publicly available data. These accession numbers for the datasets are listed in the key resources table. Differentially expressed genes in tumor cells treated with LSN3321213 and PD-L1 or LSN3321213 alone compared to vehicle from single-cell RNA-seq are included in Table S4. FPKM values from bulk RNA-seq of tumors treated with LSN3321213 compared to vehicle are included in Table S5. Cell-cycle specific gene lists are included in Table S6. Top 50 upregulated genes in G2 phase compared to M phase are included in Table S7. All data needed to evaluate the conclusions in the paper are present in the paper and/or the supplementary materials.
- This paper does not report original code.
- Any additional information required to reanalyze the data reported in this work paper is available from the lead contact upon request.

EXPERIMENTAL MODEL AND STUDY PARTICIPANT DETAILS

Mouse models

All mouse experiments complied with National Institutes of Health guidelines and were approved by Dana-Farber Cancer Institute Animal Care and Use Committee (DFCI, protocol 19-009 and 04–111). For the SCLC CRISPR-based genetically-engineered mouse

model, pure congenic Lox-stop-lox (LSL) Cas9 BL6J mice were purchased from Jackson Labs (Jackson No. 026175) and maintained as homozygous BL6J mice. Both male and female 3-4 month-old transgenic homozygous LSL-Cas9 at roughly equal numbers were used. For the 631 and 1014 syngeneic subcutaneous xenografts experiments in Figures 2 and 7, 7–9 week-old female albino B6 (C57BL/6J-Tyrc-2J, stock no. 000058; RRID:IMSR_JAX:000058) mice from the Jackson Laboratory (Bar Harbor, ME) were used. For the rechallenge experiment in Figures 7E, 16 week old female albino B6 (C57BL/6J-Tyrc-2J, stock no. 000058; RRID:IMSR_JAX:000058) mice originally from the Jackson Laboratory (Bar Harbor, ME) were used. Housing conditions for mice at the DFCI Vivarium include a 12 h/12 h day-night cycle where temperature is maintained at 72 Fahrenheit.

Cell lines

Mouse SCLC cell lines derived from our CRISPR-based SCLC GEMM including 1014 cells (male), 1015 cells (male), 159-1 cells (male), 631 cells (male) and 645 cells (male) were maintained in RPMI HITES media with 100 U/mL penicillin, and 100 μg/mL streptomycin in 37°C. Early passage cells of all cell lines listed above were tested for Mycoplasma (Lonza #LT07-218) and then were frozen using Bambanker's freezing media (Bulldog Bio). Cells were then maintained in culture for <3 months at which point new early passage vials were thawed.

DMS 79 SCLC cells (RRID:CVCL 1178) were a kind gift from Dr. Kwok-kin Wong's laboratory (New York University), and a Y chromosome was verified by QM staining and C-banding. NCI-H69 (RRID:CVCL 1579) (obtained 11/2018) were from the American Type Culture Collection (ATCC) and is from a male patient. DMS 79 and NCI-H69 cells were maintained in RPMI-1640 media with 10% FBS (Gemini) and Penicillin and Streptomycin in 37°C. All cell lines were frozen as early passage cell lines and maintained in culture for less than 6 months. Early passage cell lines were tested for Mycoplasma and were negative (Lonza #LT07-218), and then were frozen using Bambanker's freezing media (Bulldog Bio). All experiments were performed with cell lines that were maintained in culture for <6 months at which time an early passage cell lines were thawed. No commonly misidentified cell lines were used in this study.

METHOD DETAILS

Cloning adenoviral sgRNA expression vectors

Effective sgRNAs targeting mouse *Rb1*, *Trp53*, and *Rbl2* were first validated using lentiviral vectors as described previously.[22] Adenoviral sgRNA expression vectors encoding CMV-Cre recombinase and sgRNAs targeting *Rb1, Trp53, and Rbl2* and a non-targeting sgRNA was also described previously.[23] Briefly, a pENTR223-CMV-Cre-U6-sgC0111-sgRb1-sgTrp53-sgRbl2 was used in an LR recombination reaction to clone the pENTR223-U6-sgRNA vector described above into pAd-PL DEST (Invitrogen) according to the manufacturer's instructions. The recombinants were transformed into HB101 cells and ampicillin-resistant colonies were screened by restriction digestion of miniprep DNA and subsequently validated by DNA sequencing. The sgRNA oligos with BsmBI sites are specified in the key resources table.

Adenovirus production and purification

Adenoviral production and purification were performed as described previously.[23] 5 μg of the adenovirus vector (pAd/PL Invitrogen #V494-20) containing the desired sgRNA sequences and Cre recombinase expression cassette (see above) was digested with PacI (New England Biolabs) for 2 h at 37°C according to the manufacturer's instructions and column purified using Qiagen's gel extraction kit. 1 μg of PacI-digested pAd/PL was transfected into 1.5 X 10^6 293AD cells plated on a 6 cm tissue-culture dish using Lipofectamine 2000. The following day, the media was exchanged, and subsequently exchanged every 48 h thereafter. Once 293AD cells showed evidence of adenovirus production (determined by comet formation with lysis), the cells and supernatant were harvested, which were then subjected to 4 freeze-thaw cycles by alternating between an ethanol dry ice bath and 37°C. Cell debris was removed by centrifugation and the supernatant was collected, passed through a 0.45 μm filter, aliquoted, and frozen at −80°C until use.

To generate high titer adenovirus for *in vivo* experiments, adenovirus was generated as described above. 50 μL of the adenovirus stock was added to each 10 cm tissue-culture dish of 293FT cells plated at 3 X 10^6 cells per dish (4 10 cm dishes in total for each purification). When 293FT cells showed evidence of adenovirus production, as determined by cell rounding and partial detachment (~48–72 h after addition of adenoviral stock), the cells were collected, and adenovirus was purified using Virabind Adenovirus Purification Kit (Cell Biolabs #VPK-5112). The purified adenovirus was titered using QuickTiter Adenovirus Quantitation Kit (Cell Biolabs #VPK-106) according to the manufacturer's instructions.

Generation of genetically-engineered mouse models of SCLC using CRISPR/Cas9

Pure congenic Lox-stop-lox (LSL) Cas9 BL6J mice were purchased from Jackson Labs (Jackson No. 026175) and maintained as homozygous BL6J mice. Genotyping of Cas9 and GFP at the ROSA26 were confirmed for all mice on the study (Transnetyx). Both male and female 3-4 month-old transgenic homozygous LSL-Cas9 at roughly equal numbers were intratracheally injected with adenovirus (4 X 10^8 VP/mouse) encoding effective sgRNAs targeting *Rb1, Trp53, Rbl2,* and a non-targeting sgRNA (sgControl *RPR2*) and CMV-Cre recombinase. MRI of the lungs were performed on mice beginning 8 months after intratracheal injection and monthly thereafter until the mice developed tumors at which point they were randomly enrolled into one of the treatment arms (see SCLC GEMM efficacy section below).

Intratracheal injections were performed as described previously.[63] Briefly, mice were anesthetized with ketamine and xylazine and pedal reflexes were monitored to ensure adequate anesthesia. Mice were maintained on a heated stage at 37°C while anesthetized.

Mice were hung on stage with their top incisors and intubated with a 22-gauge 1 inch catheter (ThermoFisher Scientific #1484120). Once intubated, adenovirus (4 X 10^8 viral particles (VP)/mouse) in a total volume of 75 μL (diluted in PBS) was added to the catheter and subsequently inhaled by the mice.

Generation of syngeneic xenograft model in BL6 mice

The syngeneic *RPR2* 631 BL6 model was described previously.[10] Briefly, 8 X 10^6 *RPR2* 631 cells were washed 3 times in D-PBS and then resuspended in D-PBS with 50% Matrigel (Corning no. 354234) and implanted subcutaneously into 7-9 week-old female albino B6 (C57BL/6J-Tyrc-2J, stock no. 000058; RRID:IMSR_JAX:000058) mice from The Jackson Laboratory (Bar Harbor, ME). Mice with established tumors were used in the pharmacodynamic, efficacy, and flow cytometry experiments as described below. For *RPR2* 1014 syngeneic xenograft experiment, similarly 8 X 10^6 *RPR2* 1014 cells were washed 3 times in D-PBS and then resuspended in D-PBS with 50% Matrigel and injected subcutaneously injected in 7–9 week-old female albino BL6 mice. Once tumors were established, tumors were harvested and expanded *ex vivo* and reinjected into BL6 mice to establish *RPR2* 1014 P1 cells and then the process was repeated to establish *RPR2* 1014 P2 cells allowing for near 100% take rate for *RPR2* 1014 P2 cells. *RPR2* 1014 P2 cells were subsequently implanted subcutaneously into BL6 mice (C57BL/6J-Tyrc-2J, stock no. 000058) for the efficacy study. For rechallenge experiment, similarly 8 X 10^6 *RPR2* 1014 P2 cells were washed 3 times in D-PBS and then resuspended in D-PBS with 50% Matrigel and implanted subcutaneously into complete responders to LSN3321213+PD-L1 (n = 7) and age-matched naive BL6 control mice (C57BL/6J-Tyrc-2J, stock no. 000058) (n = 10).

Aurora A kinase inhibitor formulation and dosing for *In vivo* studies

LSN3321213 powder (obtained under an MTA from Eli Lilly and Company) was dissolved in 0.1 M phosphoric acid and pH was adjusted to 2.5–3.0 with sodium hydroxide. The formulation was administered twice daily (BID) by oral gavage at a dose of 57 mg/kg in a dosing volume of 5 mL/kg 0.1 M phosphoric acid was used as the vehicle throughout all studies.

Mouse MRI imaging

MRI experiments were performed on a Bruker BioSpec 7T/30-cm USR horizontal bore Superconducting Magnet System (Bruker Corp.) equipped with the B-GA12S2 gradient and integrated with a second-order room temperature shim system, which provides a maximum gradient amplitude of 440 mT/m and slew rate of 3440 T/m/s. The Bruker-made 23-mm ID birdcage volume radiofrequency (RF) coil was used for both RF excitation and receiving. The Bruker AutoPac with laser positioning was used for accurate definition of the region of interest. Animals were anesthetized with 1.5% isoflurane mixed in medical air at a flow rate of 2 L/min. Body temperature was maintained at 37°C using a warm air fan. A pressure-transducer for respiratory gating was placed on the abdomen. Animal respiration and temperature were monitored and regulated by the SAII (SA Instruments Inc., Stony Brook, NY) monitoring and gating system model 1025T. Bruker Paravision 6.0.1 was used for MRI data acquisition. T2 weighted images of the lungs were obtained using a fast spin echo (RARE) with fat suppression sequence with the following parameters: TR = 1773 ms, TE = 36 ms, Rare Factor = 8, Number of Averages = 8, total acquisition time 4 min 40 s, FOV = 24 × 24 mm2, matrix size = 192 × 256, spatial resolution = 125 × 117 μm2, slice thickness = 1.0 mm, number of slices = 20, and a total acquisition time of 7:30 min. Images were analyzed with the semi-automatic segmentation analysis software ClinicalVolumes (ClinicalVolumes, London, UK). A region of interest (ROI) delineating the tumor lesion was defined on each slice, and the total tumor volume was computed as the sum of all the ROI-defined areas.

Pharmacokinetic study in B6J mice

A pharmacokinetic (PK) study was performed to measure the plasma drug concentrations of LSN3321213 alone or LSN3321213 combined with PD-L1 antibodies in 8-week old male and female BL6J mice (Jackson no. 000664). Mice were dosed with 57 mg/kg LSN3321213 PO BID for 7 days in 0.1M H3PO4 (pH 2.5) alone or in combination with PD-L1 antibody (10F.9G2 PD-L1, Cat # BP0101, Bio X Cell) dosed at 200μg/mouse by intraperitoneally injection (IP) on days 1, 3, and 5. Two hours after the last dose, mice were euthanized and ~500μL of whole blood was collected via cardiac puncture and placed into EDTA tubes. Tubes were mixed at room temperature for 15 min then centrifuged at 7000 rpm for 7 min and plasma was collected and snap frozen in liquid nitrogen then stored at −80C and shipped on dry ice to Eli Lilly where the PK studies for LSN3321213 were performed. An aliquot of 25μL standard or plasma sample were extracted with 180 μL of a 20 ng/mL analog internal standard (proprietary Lilly compound) in methanol/acetonitrile (1:1, v/v) solution in 96-well plates. Samples were quantitated by LC−MSMS analysis using a Sprite ECHELON C18 4μm 20 × 2.1mm column (Sprite AE1822), a gradient elution and AB Sciex API 4000 triple-quadrupole mass spectrometer (Life Technologies Corporation). LSN3321213 was detected in MRM mode (490.3/206.1) at the RT (retention time) of 0.416 min and internal standard was detected in the MRM channel of 249.1/148.1 at the RT of 0.399 min. LSN3321213 concentrations were calculated via linear regression based on calibration curve using Analyst software (SCIEX).

Pharmacodynamic studies in autochthonous SCLC GEMM and *RPR2* 631 syngeneic model

For pharmacodynamic (PD) experiments in the SCLC CRISPR-based genetically engineered mouse model, both male and female homozygous BL6J LSL-Cas9 mice (Jackson no. 026175) were IT injected with sgControl *RPR2* adenovirus (see adenovirus method above). As described in generation of SCLC CRISPR GEMM model (see above), lungs MRI were performed monthly beginning 8 months after injection to detect tumors. Tumor bearing mice, confirmed by lung MRI, were treated with LSN3321213 57 mg/kg

po BID or vehicle (H_3PO_4) for 3.5 days (7 doses). Tumors were harvested 2 h after the last dose (dose 7) of LSN3321213 and snap frozen on dry ice. For the PD experiments in the syngeneic *RPR2* 631 BL6 model, the tumors were allowed to establish to 168.4 ± 13.8 mm^3 before randomization using the Studylog software (v4.2.5.8, San Francisco, CA) into vehicle control or LSN3321213 treated groups with n = 5/group using drug concentration and durations as above. Tumors were harvested 2 h after the last LSN3321213 dose and snap frozen. For each PD study, histone isolation and immunoblot analysis (see immunoblot analysis section below) was performed for phospho-histone serine 10 on histone 3 and total histone 3 to determine whether Aurora A kinase was inhibited in tumors.

SCLC CRISPR-GEMM LSN3321213 PD-L1 combination efficacy study

The efficacy study in autochthonous CRISPR-based SCLC GEMM models (see description above) was performed as follows. 3–4 month old male and female homozygous BL6J LSL-Cas9 mice (Jackson No. 026175; RRID:IMSR_JAX:026175) were IT injected with sgControl *RPR2* adenovirus (see adenovirus method above). As described in generation of SCLC CRISPR GEMM model (see above), lungs MRI were performed monthly beginning 8 months after injection to detect tumors. Once tumors were confirmed by MRI, mice were randomized to the following 4 treatment groups: 1. LSN3321213 alone dosed at 57 mg/kg po BID (by oral gavage); 2. PD-L1 antibody alone (10F.9G2 PD-L1, Cat # BP0101, Bio X Cell, used at 200μg/mouse) dosed by intraperitoneal injection (IP) three times a week; or 3. combination of LSN3321213 and PD-L1 dosed at the concentrations and frequencies above; 4. Vehicle (0.1 M H_3PO_4) dosed po BID (by oral gavage) at equal volumes compared to mice dosed with LSN3321213. Mice in all 4 treatment groups were dosed for 28 days with lung MRIs performed ∼1 day prior to treatment (day 0), 14 days after treatment, and 28 days after treatment to radiographically quantify response. After day 28, LSN3321213 or vehicle were stopped and mice in the PD-L1 or LSN3321213/PD-L1 combination groups were maintained on PD-L1 antibody for another 4 weeks as maintenance as was done in the first-line IMPOWER133 and CASPIAN human clinical trials.[3,4] After 8 weeks, all treatments were stopped and mice were monitored for survival. Body weights were measured twice a week throughout the study. Mice were euthanized when they became symptomatic defined as weight loss >15% or dyspnea and Kaplan Meier Estimator was performed to analyze survival. Upon euthanization, ∼1/2 of each lung tumor was immediately flash frozen on dry ice for subsequent RNA and protein analysis, ∼1/2 of each lung tumor and liver was fixed in 10% formalin for 24 h then stored in 70% ethanol before being embedded in paraffin. Slides were made for Hematoxylin and Eosin (H&E) and H&E slides were examined by Dr. Roderick Bronson for diagnosis.

SCLC syngeneic xenograft LSN3321213 & PD-L1 combination efficacy study

For the efficacy study in the *RPR2* 631 SCLC syngeneic model, tumors were allowed to establish to 125.6 ± 12.6 mm^3 in size before randomization into various treatment groups with 9–10 mice/group as follows: LSN3321213 was administered as above, PD-L1 antibody was administered as above; or their combinations. Vehicle control received 0.1 M phosphoric acid on the same schedule as LSN3321213. Tumor volumes were determined from caliper measurements by using the formula, Tumor volume = (length x $width^2$)/2. Tumor volumes and body weights were measured twice weekly. Mice were treated for 28 days, followed by measuring for re-growth of tumors. The experimental endpoint was when tumor volumes exceeded 2000 mm^3 at which time they were euthanized. Body weights were measured twice a week throughout the study. There were 3 mice in the LSN3321213 and PD-L1 combination arm whose tumors had a near complete response after treatment. These mice were followed for 154 days and during this time there was no re-growth of tumor. The study was terminated on day 154. Of note, during the study there was 1 mouse in the LSN3321213 and PD-L1 combination arm and 1 mouse in the single agent LSN3321213 arm that experienced weight loss of >15% by day 14. We gave a drug holiday for 1.5 days in all mice receiving any LSN3321213 treatment (alone or combo) from day 15 and re-started treatment at a lower dose of 35 mg/kg from day 17. An additional mouse in the single agent LSN3321213 treatment group experienced >15% weight loss requiring additional drug holiday for that mouse only on days 18 and 19. For the efficacy study in the *RPR2* 1014 P2 SCLC syngeneic model, mice with established tumors (>100 mm^3) were randomized ∼3:1 to LSN+PD-L1 (18 mice) vs. vehicle (7 mice) with dosing and frequency as described above. Of note, 1 mouse in the LSN3321213 + PD-L1 arm experienced weight loss of >15% by day 10 and was euthanized with pathology showing toxic changes in hepatocytes (highly vacuolated cytoplasm). At day 10, a drug holiday was given for 1.5 days in all mice and LSN3321213 treatment was re-started at 35 mg/kg BID on day 12 and continued until day 28 with no observed toxicity in any mice. There were 7 mice in the LSN3321213 + PD-L1 arm with tumors that had a complete response to treatment. 5 weeks following the completion of treatment, these mice (n = 7), together with age-matched naive BL6 mice (n = 10) were rechallenged with subcutaneous injection of 8×10^6 *RPR2* 1014 P2 cells and monitored for 45 days. During this time window, 10 of 10 naive BL6 mice formed tumors, while none of the complete responders from the LSN3321213+PD-L1 formed tumors.

To measure tumor response to treatment, adjusted AUCs were calculated using tumor volumes up to the last time point when mice were alive or had completed the full 28 days treatment course with a simple trapezoidal rule then adjusted for time[64] and log transformed to adjust the skewness,

$$adjusted\ AUC = \frac{1}{2(t_k - t_0)} \sum_{i=0}^{k-1} (\xi_i + \xi_{i+1})(t_{i+1} - t_i),$$

assuming $k+1$ measured volumes ξ_i for a tumor at time t_i (i = 0, …, k).

Complete blood count analysis

A complete blood count (CBC) analysis was performed in random SCLC CRISPR-GEMM mice enrolled in the 4-arm efficacy study after 28 days of continuous treatment to monitor toxicity. Blood was drawn by retro-orbital insertion of a Drummond hematocrit tube (Fisher Scientific # 21-171-23), collected in EDTA-coated microtainer tubes (Becton Dickinson #365973), and transferred to the Longwood Small Animal Imaging Facility (LSAIF) at the Beth Israel Deaconess Medical Center, Boston MA. Blood cell counts were determined using the MASCOT hematology profile and a HEMAVET hematology analyzer (Model 950 FS; Drew Scientific, Waterbury, CT, USA).

Generation of cell lines from mouse SCLC tumors and cell culture

Generation of SCLC cell lines from our CRISPR-based SCLC GEMM was described previously.[22,23] Briefly, LSL-Cas9 homozygous mice (described above) that grew tumors and were not enrolled into any of the studies above were euthanized and their tumors were quickly extracted, washed in ice-cold PBS, and minced several times using an ethanol sterilized razor blade. 3 mLs of collagenase/hyaluronidase (Stem cell biology #07912) diluted 1:10 in complete RPMI HITES media [10% FBS, P/S, and HITES (10 nM hydrocortisone (Sigma Aldrich #H0135), Insulin-Transferrin-Selenium (Gemini #400-145), and 10 nM beta-estradiol (Sigma Aldrich# E2257)], and 1 mL dispase (Corning # 354235) was added to the tumor and incubated at 37°C for 20–40 min (until most tumor cells were dissociated). The cells were then collected, centrifuged at 1000 rpm for 5 min, resuspended in RPMI HITES media, filtered through a 70 μm cell strainer (BD #352350), centrifuged again at 1000 rpm for 5 min, resuspended in fresh complete RPMI HITES media and placed in ultra-low adherence tissue culture dishes (Corning #3471). Media was subsequently replaced every 3 days. The cell lines were validated using immunoblot analysis for Cas9 and the SCLC neuroendocrine marker ASCL1.

sgRNA cloning and lentivirus production

sgRNA sequences were designed using the Broad Institute sgRNA designer tool (http://portals.broadinstitute.org/gpp/public/analysis-tools/sgrna-design) and synthesized by IDT technologies. The sense and antisense oligonucleotides were mixed at equimolar ratios (0.25 nmol of each sense and antisense oligonucleotide) and annealed by heating to 100°C in annealing buffer (1X annealing buffer 100 mM NaCl, 10 mM Tris-HCl, pH 7.4) followed by slow cooling to 30°C for 3 h. The annealed oligonucleotides were then diluted at 1:400 in 0.5X annealing buffer.

For CRISPR/Cas9 knockout experiments in cells, the annealed oligos were ligated into LentiGuide Puro (Addgene #52963) for experiments in mouse SCLC cell lines. Ligations were done with T4 DNA ligase for 2 h at 25°C. The ligation mixture was transformed into HB101 competent cells. Ampicillin-resistant colonies were screened by restriction digestion of miniprep DNAs and subsequently validated by DNA sequencing.

The sgRNA oligos used for LentiGuide Puro vector for CRISPR knockout experiments were specified in the key resources table.

Lentiviruses were made by Lipofectamine 2000-based co-transfection of 293FT cells with the respective lentiviral expression vectors and the packaging plasmids psPAX2 (Addgene #12260) and pMD2.G (Addgene #12259) in a ratio of 4:3:1. Virus-containing supernatant was collected at 48 and 72h after transfection, pooled together (15 mL total per 10-cm tissue culture dish), passed through a 0.45-μm filter, aliquoted, and frozen at −80°C until use.

Lentiviral infection

The cells were counted using a Vi-Cell XR Cell Counter (Beckman Coulter) and 2 $X10^6$ cells were resuspended in 1mL lentivirus with 8 μg/mL polybrene in individual wells of a 12 well plate. The plates were then centrifuged at 448 x g for 2h at 30°C. 16 h later the virus was removed and cells were grown for 72 h before being placed under drug selection. Cells were selected in puromycin (0.5 μg/mL).

Single-cell RNA sequencing experiments

The single-cell RNA sequencing (scRNA-seq) experiments in autochthonous CRISPR-based SCLC GEMM models (see description above) was performed as follows. 3–4 month old male and female homozygous BL6J LSL-Cas9 mice (Jackson No. 026175) were IT injected with sgControl *RPR2* adenovirus (see adenovirus method above). Lungs MRI were performed beginning 8 months after injection to detect tumors. Once tumors were confirmed by MRI, 9 independent mice harboring lung tumors were randomized to the following 4 treatment groups: 1. LSN3321213 (57 mg/kg po BID), mice #LSN-13 and #LSN-26; 2. PD-L1 antibody dosed at 200μg/mouse by IP three times a week, mice #PD-L1-09 and #PD-L1-25; 3. combination of LSN3321213 and PD-L1, mice #LSN+PD-L1-12, #LSN+PD-L1-18, and #LSN+PD-L1-27; or 4. Vehicle (0.1 M H_3PO_4) dosed po BID at equal volumes as LSN3321213, mice #Vehicle-14 and #Vehicle-24. Mice in all 4 treatment groups were dosed for 7 days and 2 h following the dosing on day 8, mice were euthanized and lung tumors dissected and finely minced mechanically using a razor blade and then enzymatically digested with Mouse Tumor Dissociation Kit (Miltenyi Biotec, #130-096-730) following the manufacturer's instruction. Note that vehicle-14 (mouse 168) is also included for analysis in the following study.[65] Briefly, minced tumor tissue was transferred to a gentleMACS C Tube containing enzyme mix prepared with 20% of Enzyme R option to preserve cell surface epitopes. Dissociation using the gentleMACS Octo Dissociator with Heaters (Miltenyi Biotec, #130-096-427) was performed using the 37C_m_TDK_2 gentleMACS Program. The single cell suspensions were resuspended in RPMI containing 10% FBS and subsequently passed through a 70 μm Cell Strainer (Greiner, #542070) and centrifuged at 300 x g for 3 min followed by 2 washes with 0.04% UltraPure Bovine Serum Albumin (Invitrogen, AM2616) in DPBS. Finally, dissociated cells were resuspended in DPBS with 0.04% UltraPure BSA and cell counts were measured with a Vi-CELL XR Cell Viability Analyzer (Beckman Coulter). Cells were then diluted in 0.04% BSA/DPBS at a cell concentration of

1000 cells/μL. About 16,000 cells were loaded onto a 10× Genomics Chromium instrument (10× Genomics) according to the manufacturer's instructions. The scRNA-seq libraries were processed using Chromium Next GEM Single Cell 5′ Kit v2 kit (10× Genomics). Quality controls for amplified cDNA libraries and final sequencing libraries were performed using Bioanalyzer High Sensitivity DNA Kit (Agilent). The sequencing libraries for scRNAseq were normalized to 4 nM concentration and pooled. The pooled sequencing libraries were sequenced on Illumina NovaSeq S4 300 cycle platform. The sequencing parameters used were: Read 1 of 26bp, Read 2 of 90bp, Index 1 of 10bp and Index 2 of 10bp.

Single-cell RNA sequencing data analysis

Custom reference genome was established by adding EGFP and Cas9 sequence[66] to the mouse genome (mm10-2020-A). Cell ranger version 6.0.2 pipeline (10× Genomics) was used to align sequencing data to the custom mouse reference genome and generate the gene-level counts matrix. Unfiltered raw counts data was imported into Seurat v4 R package (version 4.1.0)[61] for downstream processing and analysis. Low quality cells were filtered out using following thresholds: total UMI counts <500, number of transcripts <350, $\log_{10}$TranscriptsPerUMI $\leq$ 0.8, and cells with more than 15% mitochondrial genes. In addition, genes expressed in less than ten cells were removed. The UMI counts matrices were then natural-log normalized and scaled with Seurat's NormalizeData and ScaleData functions.

Dimension reduction, cluster analysis and visualization of scRNA-Seq data

The Seurat v4 R package was used for dimension reduction and clustering. Top 2,000 genes with the highest variance were selected using the 'FindVariableFeatures' function with 'vst' method to perform linear dimensional reduction (principal component analysis) using the 'RunPCA' function, and top 40 principal components were used to perform graph-based unsupervised clustering with the 'FindNeighbors' and 'FindClusters' functions and Uniform Manifold Approximation and Projection for Dimension Reduction (UMAP) (arXiv:1802.03426) for data visualization in two-dimensional space. The R package SingleR (version 1.8.1)[67] was used for automatic cluster annotation with ImmGenData.[68,69] Automatic cluster annotation was validated and curated based on established marker gene expression (Figures 4A, S6C, and S9B). After cluster annotation, tumor cells expressing *Ptprc* and *Pecam1*, immune cells expressing *Epcam*, *Pecam1*, and *Cas9*, Fibroblast expressing *Epcam*, *Pecam1*, *Cas9*, and *Ptprc*, endothelial cells expressing *Epcam*, *Cas9*, and *Ptprc*, and AT2/club cells expressing *Cas9* were filtered out to exclude potential doublets. Next, subpopulations were reanalyzed separately by repeating the procedure described above. Seurat's CellCycleScoring function was used to identify the cell cycle phases based on cell-cycle specific gene expression (Table S6) and manually categorization of M and G2 population was done using a gene-set of known cell cycle genes (Table S7).[60,70] To calculate the IFNγ target gene score, Seurat's AddModuleScore function was used on the following genes: *B2m, Cd74, Birc5, Scgb1a1, Ucp2, Spp1, Ftl1, Krt10, Casp8, and Hmox1,* which are the top 10 prioritized ligand targets based on regulatory potential of IFNγ. Differentially expressed genes were calculated with the Wilcoxon test of Seurat's 'FindMarkers' function with default settings, to compare differentially expressed genes between clusters. R package ClusterProfiler (version 4.2.2)[71] was used in Gene Set Enrichment Analysis (GSEA) of scRNA-seq differential expressed genes analysis and R package EnhancedVolcano (version 1.12.0) was used in volcano plotting of differentially expressed genes.

Superimposing tumor datasets between treatment groups with scRNA-seq data

In order to recover sharper biological distinction, each treatment group was transformed using the 'SCTranform' function in Seurat v4. In the 'SCTransform', number of UMI and mitochondrial gene percentage were regressed out using the 'var.to.regress' option. Then, top 3000 variant genes in each treatment group were selected as variable features for integration. The cell pairwise correspondences among treatment groups, called 'anchors', were identified using 'FindIntegrationAnchors' function followed by integration between treatment groups with the 'IntegrateData' function by transforming the datasets into a shared space.

Tumor and its Microenvironment Communication Analysis using differential NicheNet of scRNA-Seq data

To study communication between the tumor and cells of the microenvironment in different treatment conditions, we applied an established method known as nichenetr package V 1.1.0.[39] NicheNet predicts which differentially expressed ligands from one tumor microenvironment population are most likely to affect target gene expression of tumor population and which specific target genes are affected by which of these predicted ligands. It uses ligand-receptor and ligand-target databases as references to evaluate the cellular communication networks between two cell types. Human gene names were converted to their one-to-one orthologs using 'convert_human_to_mouse_symbols' function. Ligands, receptors, and targets that expressed in at least 10% (default cutoff) of the single cells in a specific cluster were included. Differential genesets of interest were calculated using a log transformed fold change threshold of 0.15 (recommended cutoff for 10x datasets), and 495 genes were included in vehicle and 1022 genes of interest were included in combination treatment group. Next, ligand-receptor-target links were prioritized using the weights of scaled properties of interest as follows: "scaled_ligand_score" = 5, "scaled_ligand_expression_scaled" = 1, "ligand_fraction" = 1, "scaled_ligand_score_spatial" = 0, "scaled_receptor_score" = 0.5, "scaled_receptor_expression_scaled" = 0.5, "receptor_fraction" = 1, "ligand_scaled_receptor_expression_fraction" = 1, "scaled_receptor_score_spatial" = 0, "scaled_activity" = 0, "scaled_activity_normalized" = 1, "bona_fide" = 1.

Bulk RNA-Sequencing of autochthonous mouse SCLC tumors

The same tumor samples from the SCLC CRISPR GEMM PD study described above were used to perform bulk RNA-sequencing. Briefly, tumors were harvested at necropsy and were flash-frozen. RNA was extracted using RNeasy mini kit including a DNase

digestion step according to the manufacturer's instructions and RNA-sequencing was performed. Total RNA samples in each experiment were submitted to Novogene Inc. The libraries for RNA-seq are prepared using NEBNext Ultra II non-stranded kit. Paired end 150bp sequencing was performed on Novaseq6000 sequencer using S4 flow cell. Sequencing reads were mapped to the mm10 genome by STAR. Statistics for differentially expressed genes were calculated by DESeq2. For Gene Set Enrichment Analysis (GSEA), software was downloaded from the Gene Set Enrichment Analysis website [http://www.broad.mit.edu/gsea/downloads.jsp]. GSEA was performed using the 'Hallmark' gene sets. Gene Sets with an FDR<0.25 were considered significant. For principal component analysis and cluster analysis, top 500 genes in terms of the largest standard deviation were subjected to principal component analysis using the prcomp function of R software, and the first two components were plotted.

Flow cytometry of SCLC mouse xenograft tumors

See method for Generation of *RPR2* 631 Syngeneic Xenograft Model in B6 Mice above. Using our *RPR2* 631 syngeneic xenograft model, tumors were allowed to establish to 129.2 ± 25.8 mm^3 in size before randomization into various treatment groups (see syngeneic model efficacy study method for treatment groups) with 6 mice/group. Mice were treated for 7 days under the different treatment conditions with the same treatment doses and duration as in the scRNA-seq experiment in our CRISPR-based SCLC GEMM (see method above). 2 h following the last dose, fresh tumors were enzymatically disaggregated in C-tubes (Miltenyi) in dissociation buffer consisting of RPMI (Life Technologies) +10% FBS (HyClone), 100 U/ml collagenase type IV (Life Technologies), and 50 μg/mL DNase I (Roche). Suspension was incubated at 37°C for 45 min and then further mechanically dissociated on OctoMACS Separator (Miltenyi). Red blood cells were removed from samples using red blood cell lysis buffer (Biolegend). Samples were pelleted and then resuspended in fresh RPMI +10% FBS and strained through a 40 μm filter. Cells were incubated with the Live/Dead Zombie NIR (Biolegend) for 5 min in the dark at room temperature. Fc receptors were blocked prior to surface antibody staining using mouse FcR Blocking Reagent (Biolegend). Cells were stained for 15min on ice in the dark and washed 2x with PBS +2% FBS. Cells were fixed, permeabilized, and stained with intracellular antibodies using Foxp3/Transcription Factor Staining kit according to manufacturer's protocol (eBioscience). Cells were analyzed on a BD LSRFortessa with FACSDiva software (BD Biosciences). Data was analyzed using FlowJo software version 10.5.3. Antibodies were specific for the following mouse markers: CD44-Alexa488 (IM7), CD49b-PerCp/Cy5.5. (DX5), CD8-PE/Dazzle (53-6.7), CD3-Alexa700 (17A2), PD-1-BV421 (RMP1-30), CD45-BV510 (30-F11), CD62L-BV570 (MEL-14), CD19-605 (6D5), CD4-BV711 (GK1.5), Ly6C-FITC (HK1.4), Ly6G-PerCp/Cy5.5 (1A8), CD68-PE/Cy7 (FA-11), PD-L1-BV421 (10F.9G2), CD11c-BV570 (N418), CD11b-BV711 (M1/70), and F4/80-BV785 (BM8) from Biolegend.

Growth inhibition assays

Mouse SCLC cells were plated in complete media (see above) in 6-well plates containing 2 mL of media per well at the following cell densities at 200,000/mL at various concentrations of LSN3321213 or DMSO. Cells were harvested 72 h later, centrifuged at 434 x g for 3 min, resuspended in 1 mL of trypsin to make single cell suspensions, and counted using a Vi-Cell XR Cell Counter (Beckman Coulter). Cell counts were then normalized to the DMSO condition.

B2m RT-qPCR or MHC class I flow cytometry after LSN3321213 and/or IFNγ in SCLC Cell lines

1014 and 645 cells were counted on the Vi-Cell Counter and plated at 100,000 cells/mL in either LSN3321213 (125 nM) or DMSO. 48 h later, IFNγ (10 ng/mL) was added to the cells where indicated. 20 h later, cells were harvested to make RNA for RT-qPCR for *B2m* or (in separate independent experiments) stained for MHC class I for flow cytometry analysis.

NCI-H69 and DMS 79 human SCLC cell lines were plated at 400,000 cells/ml with DMSO, LSN3321213 (125 nM), IFNγ (10 ng/mL), or LSN3321213 (125 nM) +IFNγ (10 ng/mL). 24 h later, cells were stained for MHC class I for flow cytometry analysis.

Reverse-transcriptase quantitative PCR (RT-qPCR)

RNA was extracted using RNeasy mini kit (Zymo Research #R1055) according to the manufacturer's instructions. RNA concentration was determined using the Nanodrop 8000 (Thermofisher Scientific). A cDNA library was synthesized using iScript Reverse Transcription Supermix for RT-qPCR (Biorad # 1708841) according to the manufacturer's instructions. qPCR was performed using the SYBR Green I (BioRad #1725271) and oligos below according to the manufacturer's instructions. The DDC_T Method was used to analyze data. The C_T values for each probe were then normalized to the C_T value of *36b4* for that sample. The data from each experiment was then normalized to the control to determine the relative fold change in mRNA expression. The SYBR Green primer oligonucleotides were specified in the key resources table.

FACS-based MHC class I surface expression

Live cells were centrifuged at 400 x g, washed once in PBS, centrifuged again at 434 x g, and then washed again in PBS containing 2% FBS (FACS buffer). For mouse cell experiments, cells were centrifuged again at 434 x g and stained with anti-mouse H-2L^d/H-2D^b PE (Biolegend #114507), Pacific Blue anti-mouse H-2K^b (Biolegend #116514), APC anti-mouse H-2K^b bound to SIINFEKL (Biolegend #141606), or the corresponding IgG isotype control (Biolegend 400211, 400235, 400119) diluted at 1:100 in FACS buffer and incubated for 30 min in the dark at room temperature. For human cell experiments, cells were centrifuged again at 434 x g and stained with PE anti-human HLA-A,B,C Antibody (Biolegend #311406), or the corresponding IgG isotype control (Biolegend #400214) diluted at 1:100 in FACS buffer and incubated for 30 min in the dark at room temperature. Cells were then washed again in FACS buffer,

centrifuged, and finally resuspended in FACS buffer and analyzed on a BD-Fortessa collecting data from at least 10,000 cells per sample per replicate. Live cells were first gated, doublets were then excluded, and MHC class I was then collected using the isotype as a control. Flow Jo was used for analysis and the fold increase compared to IFNγ alone was calculated.

Immunoblot analysis

Mouse SCLC cells above were centrifuged at 400 x g for 3 min at 4°C and the media was removed by gentle aspiration. The cell pellet was then washed once in 1 mL of ice-cold PBS, transferred to a 1.5 mL Eppendorf tube, and centrifuged at 400 x g for 3 min at 4°C. The PBS was carefully aspirated and the cell pellet was lysed in EBC lysis buffer (50mM Tris Cl pH 7.5, 250 mM NaCl, 0.5% NP-40, 10% Glycerol) supplemented with a protease inhibitor cocktail (Complete, Roche Applied Science, #11836153001) and phosphatase inhibitors (PhosSTOP Sigma #04906837001). Soluble cell extracts were quantified using the Bradford Protein Assay. 40 μg of protein per sample was boiled in sample buffer (3X is 6.7% SDS, 33% Glycerol, 300 mM DTT, and Bromophenol Blue), resolved by SDS-polyacrylamide gel electrophoresis (SDS-PAGE) (10% SDS-PAGE for phospho-Aurora kinase), transferred onto nitrocellulose membranes, blocked in 5% milk in Tris-Buffered Saline with 0.1% Tween 20 (TBS-T) for 1 h, and probed with the indicated primary antibodies overnight at 4°C. Membranes were then washed 3 times in TBS-T, probed with the indicated horseradish peroxidase-conjugated (HRP) secondary antibodies for 1 h at room temperature, and washed 3 times in TBS-T. Bound antibodies were detected with enhanced chemiluminescence (ECL) western blotting detection reagents [Immobilon (Thermo Fisher Scientific, #WBKLS0500) or Supersignal West Pico (Thermo Fisher Scientific, #PI34078)]. The primary antibodies used were: rabbit α-phospho-Aurora A/B/C (Cell Signaling #2914, used at 1:1000), rabbit α-MASH1/Achaete-scute homolog 1 antibody (Abcam, EPR19840, used at 1:1000), rabbit α-TAP1 antibody (Cell Signaling #12341, used at 1:1000) mouse α-Vinculin (Sigma, hVIN-1, #V9131 used at 1:1000), and mouse α-β-actin (Sigma, clone AC-15, #A3854, used at 1:25,000). The HRP conjugated secondary antibodies were Goat α-Mouse and Goat α-Rabbit (Jackson Immuno Research) and were used at 1:5000.

For immunoblot analysis of histones, tumors were finely minced mechanically and then resuspended in Nucleus Lysis Buffer (250 mM Sucrose, 60 mM KCL, 15 nM NaCl, 15 mM Tris pH 7.5, 5 mM $MgCl_2$, 1 mM $CaCl_2$, 1 mM DTT, 0.3% NP-40 supplemented with a cocktail of protease inhibitor cocktail and phosphatase inhibitors) and incubated at 4°C for 10 min. The extracts were then centrifuged at 10,000 x g for 1 min at 4°C and the supernatant was removed by aspiration. The cell pellets were again resuspended in Nucleus Lysis Buffer and incubated for 10 min at 4°C and then centrifuged at 10,000 x g for 1 min at 4°C. The supernatant was removed by aspiration and the histones in the insoluble pellet were extracted by overnight incubation in 100 μL of 0.2 N HCl followed by centrifugation at 16,800 x g for 15 min at 4°C. The supernatant was transferred to a fresh 1.5 mL Eppendorf tube and quantified using the Bradford Protein Assay. The pH of the supernatant was neutralized by adding 1/5 volume of 1 N NaOH, as confirmed by the color of the samples after the addition of sample buffer containing Bromophenol Blue. 1 μg of protein in sample buffer was boiled and resolved by SDS-polyacrylamide gel electrophoresis on a 15% SDS-PAGE gel. Immunoblot analysis was performed as described above. The primary antibodies used were: rabbit α-Histone 3 (Cell Signaling, DH12, #4499), and rabbit α-Phospho-Histone H3 Serine 10 (Cell Signaling, #9701). The secondary antibody was HRP-conjugated Goat α-Rabbit (Pierce).

Ovalbumin–luciferase transduction and OT-I T cell Co-culture assay

RPR2 1014 cell lines were transduced with the pLVX–lucOS–IRES–Neo lentiviral vector to stably express OVA antigen.[72] Cd8a+ T cells were isolated from 8- to 12-week-old C57BL/6-Tg (TcraTcrb)1100Mjb/J OT-I mice (stock 003831; Jackson Laboratory; RRID:IMSR_JAX:003831) using magnetic beads separation and LS columns following the manufacturer's protocol (cat. 130-049-401; Miltenyi Biotec). OT-I T cells were activated with Dynabeads Mouse T-Activator CD3/CD28 beads (cat. 11456D; Thermo Fisher Scientific) for 24 h before co-culture experiments were performed. *RPR2* 1014 OVA cells were pretreated with DMSO or LSN3321213 (125 nM) for 72 h with IFNγ (10 ng/mL) stimulation for 16 h where indicated. Then tumor cells (target) were washed once with PBS to remove IFNγ, replenished with LSN3321213 (10 ng/mL) where indicated and seeded in 10,000 cells/well density on 96-well plates and co-cultured with activated OT-I Cd8a+ T cells (effector) at effector-to-target (E/T) ratios of 0:1, 1:1, 2:1 for 48 h. Tumor cell survival was measured by luminescence as previously described.[72] Percent survival was calculated by dividing luminescence of each E/T ratio by luminescence of corresponding tumor cell conditions without T cells.

Gene set enrichment analysis (GSEA) and gene set variation analysis (GSVA) of RNA-seq data

GSEA software was downloaded from the Gene Set Enrichment Analysis website [http://www.broad.mit.edu/gsea/downloads.jsp]. GSEA was performed using Hallmark gene sets, antigen processing and presentation of peptide antigen gene set (#0048002) from GO Biological Processes gene lists, top 50 upregulated genes in G2 phase vs. M phase,[60] and ASCL1 target gene list[73] in Figures 5, 6, S9, S11, and S15.

R package GSVA (1.48.3) was used to calculate antigen presentation machinery score based on expression of *B2M*, *TAP1*, and *TAP2* by "gsva" function with default parameters in Figures S1A and S1B.

QUANTIFICATION AND STATISTICAL ANALYSIS

For the *in vivo* studies in the autochthonous SCLC mouse models and SCLC syngeneic models, Gehan-Breslow-Wilcoxon test was used to determine the p value of the Kaplan-Meier survival analysis. Fisher's exact test was used to calculate statistical significance

for the contingency tables in Tables S1 and S2. For the body weight curves of *in vivo* studies in the autochthonous SCLC mouse models and SCLC syngeneic models, a mixed effect model was fitted to determine the significance of the treatment induced body weight difference. For comparing normalized read counts of *B2m* in different treatment groups and cell cycle phases in the scRNA-seq analysis, non-parametric two sample Kolmogorov-Smirnov test were used. For the bulk RNA-sequencing experiments, statistical significance was calculated using FDR corrected for multiple hypothesis testing where q-value of <0.25 is considered statistically significant. For the RT-qPCR experiments, statistical significance was determined by calculating p value with the ratio paired t test. For all other experiments, statistical significance was calculated using unpaired, two-tailed Student's *t* t-test. p values were considered statistically significant if the p value was <0.05. For all figures, * indicates p value < 0.05, ** indicates p value < 0.01, *** indicates p value < 0.001, and **** indicates p value < 0.0001. Error bars represent SEM unless otherwise indicated. Additional statistical details of experiments can be found in the figure legends. Samples were always randomly allocated to experimental groups. All homozygous LSL-Cas9 mice (both male and female at roughly equal numbers and hence the results were not influenced by gender) were randomly assigned to receive adenovirus and/or treatments. All BL6J mice in syngeneic xenograft studies were randomly allocated to experimental treatment groups. For the CRISPR-based SCLC autochthonous GEMM experiments in Figure 1, the investigators performing and analyzing the lung MRIs were blinded to the treatment group. For scRNA-seq and bulk-seq experiments, the investigators that processed and sequenced the samples [DFCI TIGL core (scRNA-seq), or Novogene (RNA-seq)] were blinded to the identity of the samples. For *in vitro* experiments, same cell lines from the same maintenance culture were infected with the indicated sgRNAs at the same time for each biological independent experiment and biological independent experiments were performed on different days. For all experiments, no data were excluded from any analyses.